Liposomal formulation of an emetine analog in combination with daunorubicin for the treatment of acute myeloid leukemia

This thesis is submitted in partial fulfillment of the requirements for the degree of Master of Pharmacy

By

Tuva Torblå Bakke

Centre for Pharmacy and Department of Clinical Science

University of Bergen, Norway

May 2019

2019

Liposomal formulation of an emetine analog in combination with daunorubicin for the treatment of acute myeloid leukemia

Acknowledgements

I would like to acknowledge and thank the following individuals and groups for their contributions and support.

My supervisor Prof. Lars Herfindal for all his guidance, encouragement, thorough read throughs and for answering all my questions.

Dr. Reidun Æsøy and Edvin Tang Gundersen, MSc., for all their help and for sharing their knowledge. The other members of the group and the PhD-candidates of the 9th floor for dropping by my "office" and offering support.

Dr. Fabrice Anizon at the University of Clermont Auvergne for letting me study the emetine analog, FG1181.

My fellow nanotechnology bachelor students and pharmacy master students for their support and company over the years, and especially Bendik Auran Rathe this last year for his encouragement during long hours at the lab.

My colleagues, friends and family, and especially my parents and siblings. Thank you all for being so supportive and understanding.

Thank you for the proof reading to my brother, Torstein Bakke Torblå, his girlfriend Sabrina Parizadeh and Krister Joakim Trandal.

Finally, I want to thank my fiancé Ørjan Augedal for his never-ending love, and for not letting me give up.

Thank you,

Tuva Torblå Bakke

Table of contents

Acknowledgements....3

Table of contents....4

Abbreviations....7

Abstract....9

1. Introduction....10

1.1. Acute myeloid leukemia....10

1.2. Nanosized drug delivery systems....15

1.2.1. Liposomes....17

1.3. Choice of compounds....18

1.3.1. Anthracyclines....19

1.3.2. Emetine and analogs....21

1.4. Aims....22

2. Experimental theory....23

2.1. Spectroscopy....23

2.1.1. Dynamic light scattering....23

2.1.2. Infrared spectroscopy....24

2.2. Western blotting....25

2.3. Chromatography....26

2.3.1. Size exclusion chromatography....26

2.3.2. High-performance liquid chromatography....27

2.4. Membrane permeability 28

2.5. Assessment of cellular cytotoxicity 29

2.5.1. Cell lines 29

2.5.2. Assessment of cell viability 30

3. Materials and methods 32

3.1 Materials and reagents 32

3.2 Equipment and instrumentation 33

3.3 Production of liposomes 34

3.3.1 Preparation of liposomes 34

3.3.2 Compound loading of liposomes 35

3.3.3 Reverse phase high performance liquid chromatography 35

3.4 Parallel artificial membrane permeability assay 36

3.5 Cell maintenance and experiments 37

3.5.1 Cell maintenance 37

3.5.2 Metabolic activity measurements 37

3.5.3 Kinetics assay 38

3.6 Protein detection 38

3.7 *In silico* prediction, data analysis and presentation 40

4 Results 41

4.1 FG1181 chemical properties and anti-AML activity 41

4.2 Liposomal formulations 47

4.2.1 Liposomal characteristics 48

4.2.2 Compound loading of liposomes 50

4.2.3 Pulse test 55

5 Discussion 57

6 Concluding remarks and further investigations 63

References 64

Appendix I - Western blotting results 73

Appendix II – RP-HPLC spectra of FG1181 and daunorubicin loaded liposomes 74

Abbreviations

ACN	Acetonitrile
ALL	Acute lymphatic leukemia
AML	Acute myeloid leukemia
AML-MRC	Acute myeloid leukemia with myelodysplasia-related changes
ara-C	Cytarabine
AUC	Area under the concentration-time curve
Chol	Cholesterol
DDS	Drug delivery system
DLS	Dynamic Light Scattering
DMEM	Dulbecco's modified Eagle's medium
DMSO	Dimethyl sulfoxide
DNA	Deoxyribonucleic acid
DNR	Daunorubicin
DOX	Doxorubicin
DSPE-PEG	1,2-Disteraoyl-sn-glycero-3-Phosphoetanolamine-N-[Methoxy(Polyethylene glycol)-2000]
DSPE-PEG(5000)folate	1,2-distearoyl-sn-glycero-3-phosphoethanolamine-N-[folate(polyethylene glycol)-5000] (ammonium salt)
EME	Emetine
EPR effect	Enhanced permeability and retention effect
FAB	French-American-British
FBS	Fetal bovine serum
Fix	Formaldehyde and 100 µL Hoechst 33342 in PBS
H9c2	Rattus norvegicus heart/myocardium myoblast cells
HEPC	Hydrogenated egg phosphatidylcholine
HPLC	High-performance liquid chromatography
HSCs	Hematopoietic stem cells
IDA	Idarubicin

IR	Infrared
LS-MC	Liquid chromatography-mass spectroscopy
LMV	Large multilamellar vesicles
LSC	Leukemia stem cell
MQ	Milli Q
NC	Nanocarrier
NRK	Rattus norvegicus kidney fibroblast cells
PAMPA	Parallel artificial membrane permeability assay
PBS	Phosphate buffered saline
PdI	Polydispersity Index
PEG	Poly(ethylene glycol)
RP-HPLC	Reverse phase high performance liquid chromatography
SEC	Size exclusion chromatography
t-AML	Therapy related acute myeloid leukemia
TBS	Tris buffered saline
TBS-T	1% Tris buffered saline and 1% Tween in MQ
TFA	Trifluoroacetic acid
TG	Tris/Glycine Buffer
TGS	Tris/Glycine/SDS Buffer
UV	Ultraviolet
WHO	World Health Organization
WST-1	Water soluble tetrazolium salt

Abstract

The anthracycline drug daunorubicin (DNR) is, together with cytarabine, the most commonly used chemotherapeutic agents against acute myeloid leukemia (AML) and has been so for the last 40 years. AML is a disease with low survival rate, and is most common among the elderly with a median age of diagnosis at around 70 years. The current treatment method is impaired by low tolerance and severe dose-related side-effects, including myelosuppression. Improved treatment methods, especially for frailer patients, are needed.

Previous studies has shown that the combination of a protein synthesis inhibitor (cycloheximide or emetine (EME)) with DNR is shown to act synergistic in inducing AML cell death. Furthermore, by introducing EME 30 minutes after DNR, the anti-AML effect was further enhanced. By incorporating EME and DNR in a dual-compound liposome, equal pharmacokinetics of the compounds and simultaneous release at the target are ensured. Incorporating anthracyclines in liposomes has shown to lower side-effects of the drugs, thus improving the current treatment method.

An EME analog, FG1181, was developed in order to ensure sequential drug delivery to cells. FG1181 is expected to be metabolized into EME after 20-30 minutes, thus ensuring the advantageous delayed protein synthesis inhibition after exposure to DNR. This thesis presents the documentation of FG1181 with respect to chemical properties, cytotoxicity, and also the development of a method for producing liposomes loaded with both FG1181 and DNR. We demonstrate that FG1181 is less potent towards AML cells compared to EME, and has delayed toxic effect. Furthermore, the compound can be loaded into liposomes with a modified acid precipitation method, using incubation at low temperatures to prevent hydrolysis of FG1181 into EME during production of liposomes.

Finally, we found that liposomes loaded with FG1181 and DNR had higher anti-AML activity than liposomes loaded with EME and DNR, suggesting that the advantageous effect of sequential drug delivery is obtained by the prodrug concept. In conclusion, small molecules, here loaded into liposomes, are promising in the field of cancer therapy and can be expected to improve the treatment of AML.

1. Introduction

1.1. Acute myeloid leukemia

Leukemia is a group of cancerous diseases defined by chromosomal translocation or mutation in the hematopoietic stem cells (HSCs) lineage (1, 2). During normal hematopoiesis, HSCs mature into different blood cells in the lymphoid and myeloid cell lineage, as illustrated in Figure 1.1 (3, 4). However, the leukemia stem cells (LSCs) do not lead to proliferation of healthy blood cells like their non-mutated counterparts HSCs (5). LSCs have terminated differentiation, meaning that there will be an accumulation of immature precursor cells, termed blasts, in the bone marrow and peripheral blood, or other hematopoietic or lymphoid organs (6).

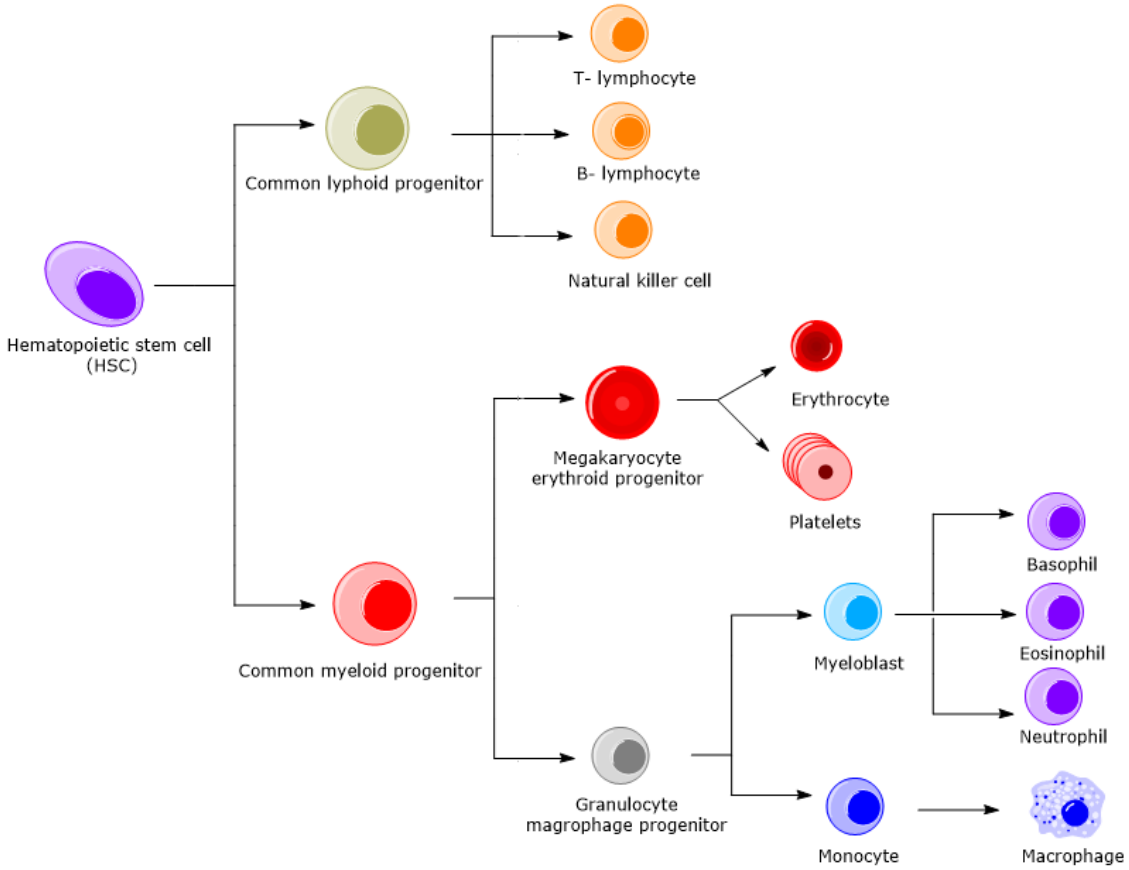

Figure 1.1 - The process of hematopoiesis. The figure illustrates the different lineages in hematopoiesis for HSCs. The red figure farthest to the left represents the common myeloid progenitor. Mutations in this progenitor could lead to myeloid leukemia, while mutations in the green lymphoid progenitor can lead to lymphoid cancers. Figure adapted from Lara and George (7).

Leukemia is classified based on the degree of blast proliferation and morphological differentiation, and on the clinical course of the patients (5, 8). Acute leukemia is mutations in the most immature precursor cells, characterized by a high degree of proliferation, lack of morphological differentiation, and rapid disease progress (4, 8). Acute leukemia develops rapidly during weeks or months, and requires immediate medical treatment (9). Chronic leukemia cells, on the other hand, derive from more mature blast cells. It is characterized by a low proliferation rate, slower clinical development, and accumulation of nonfunctional cells resisting apoptosis (1, 8).

Acute leukemia leads to hematopoietic insufficiency because of the rapidly multiplying blasts consuming the nutrients and space in the blood marrow intended for normal hematopoiesis (8, 10). This results in deficient production of erythrocytes, leukocytes and thrombocytes, causing insufficient oxygen transport, leading to perceptible symptoms like fatigue, shortness of breath, anemia and bone pain (8, 11). Other symptoms include cold sores or gingivitis, frequent infections, weight loss and fever of unknown origin, caused by the immune system being impaired by a subnormal level of leukocytes (11). An increase in hematomas and bleeding is caused by an insufficient number of thrombocytes.

Half a century ago, acute leukemia was considered incurable and palliative care was the only option (3). Today there is multiple treatment methods depending on subclassification of the disease. Acute lymphatic leukemia (ALL) entails mutations in lymphoblasts line illustrated as green in Figure 1.1 and is the most common type of leukemia in children aged 0-19 (12). This thesis will focus on acute myeloid leukemia (AML), a condition with mutations in the most immature myeloblast line illustrated as red in Figure 1.1 (4). AML is the second most common type of leukemia for adults, and the most common acute leukemia for patients aged 20 years and over (4).

Every year around 200 patients are diagnosed with acute leukemia in Norway, where 160 of these are AML (11). In the United States of America (USA), it was estimated that around 19,520 new patients would be diagnosed in 2018, of which 10,670 would die as a result of the disease (12). Figure 1.2 shows the age distribution and incidence rate per 100,000 for diagnosis per year in the United Kingdom (UK), which is comparable to Norway (13). The figure shows that the incidence rate per 100,000 is higher for men compared to women. In the US, the median age for patients diagnosed with AML is 67 years and 75% of newly diagnosed patients are older than 60 years (4, 14, 15). As life expectancies in Norway have increased with 5 years for

women and 8 years for men in the last 30 years, it becomes apparent that an increase in AML incidences can be expected (16).

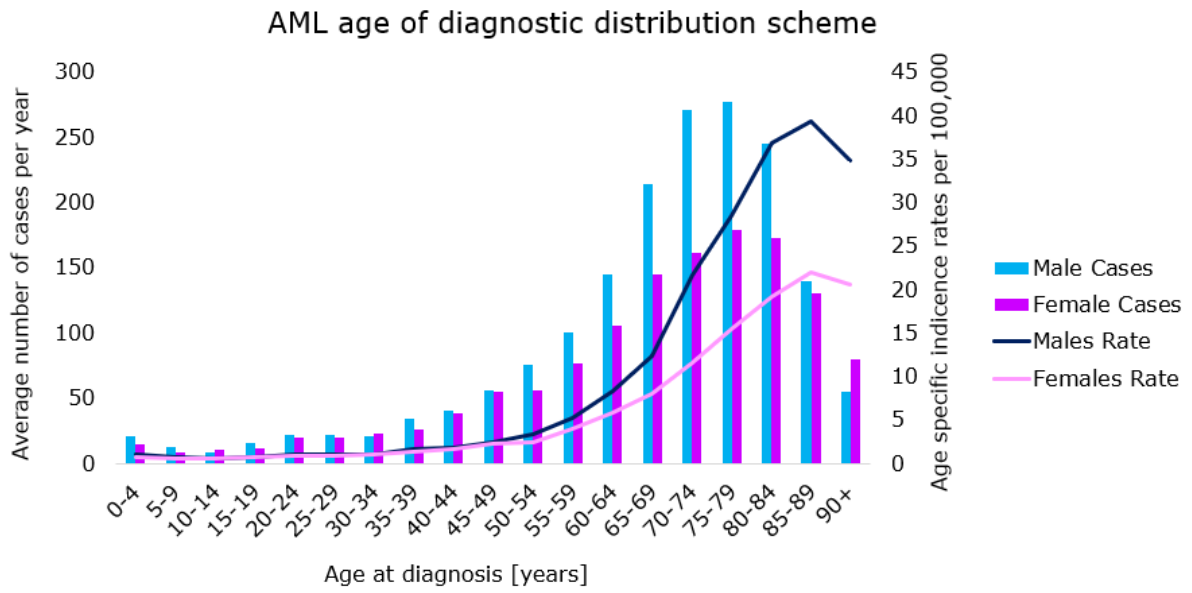

Figure 1.2 – Age distribution of AML diagnosis. The figure indicates time of AML diagnosis separated by age and gender. The vertical columns indicate the number of diagnosis per year relative to the left y-axis. The incidence rate per 100,000 for age and gender is illustrated as continuous lines relative to the y-axis on the right side. The numbers are based on data for 2013-2015. Figure adapted from Cancer Research UK (13).

The American Cancer Society assume a 24% overall survival rate of five years for adults diagnosed with AML (12). The European Union estimates a 5-year survival rate of 19%, with 3-8% for patients aged ≥ 60 years, which is significantly less than for other cancer types (14, 15, 17). Figure 1.3 shows disease and age dependent survival prognosis based on the National Cancer Research Institute of UK and the Swedish Acute Leukemia Registry (18, 19). The patients' diseases are classified as favorable, intermediate or adverse based on factors like cytogenetics and blast differentiation status (20, 21). The graphs clearly indicate the need for improved treatment methods, especially for the patients of higher age and in the adverse group. Patients not receiving treatment usually die within weeks or months from sequelae infection or bleeding (22, 23).

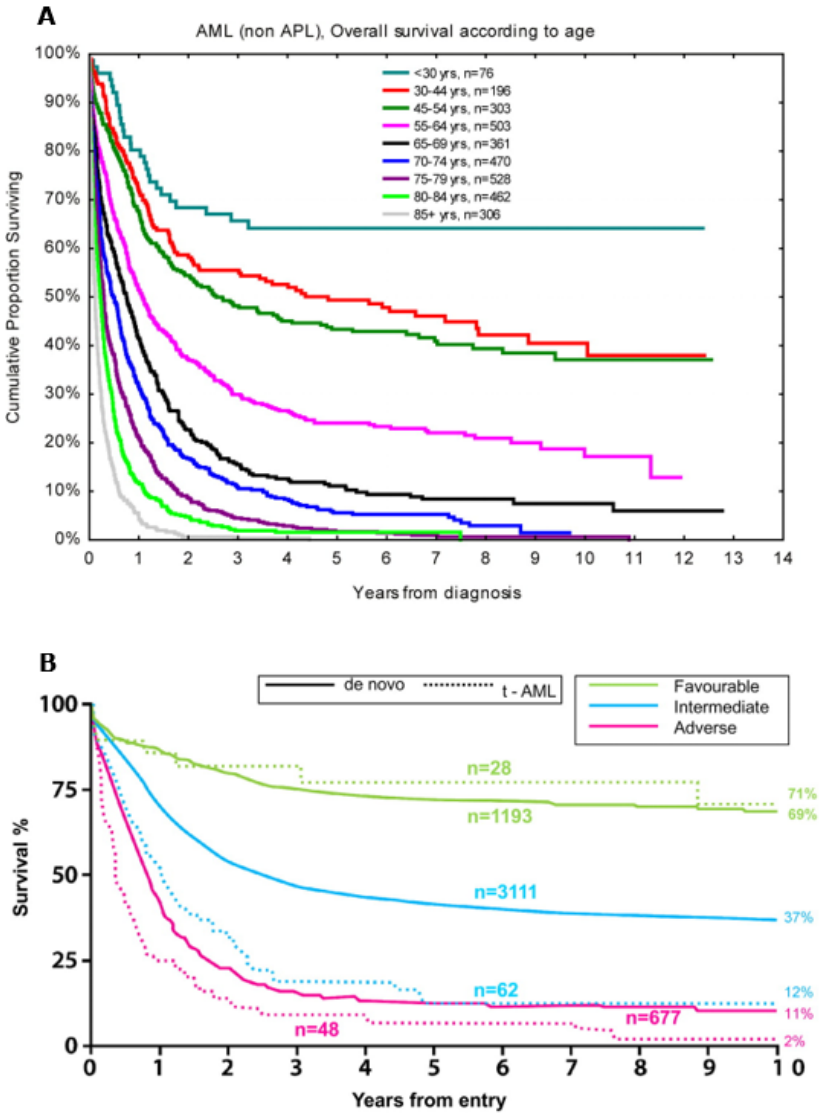

Figure 1.3 – Survival prognosis of patients with AML based on age and disease characteristics. A, Overall survival according to age for AML patients. The data was collected from the Swedish database of diagnosis between 1997 and 2006, with follow up in 2008. Note the low survival rate for patients aged 65 years and older. Figure taken from Juliusson, Lazarevic (18). **B,** Survival rate based on disease characterized as favorable, intermediate or adverse for patients aged 16-59 in the UK. *De novo* is new mutation AML while therapy related acute myeloid leukemia (*t-AML*) showed in the scheme is AML caused by previous treatment with chemotherapy or radiation therapy. Figure adapted from Grimwade and Hills (24) and taken from Rowe and Tallman (19).

The recommended treatment will be partly based upon which subgroup or genetic variation of the disease the patient is diagnosed with, according to classifications defined by the French-American-British (FAB) or the World Health Organization (WHO) (25, 26). An example of one of the eight subgroups defined by FAB is an AML classified as AML FAB M5a, represented in this thesis by the cell line MOLM13 (22). MOLM13 was collected from a human

20-year-old male diagnosed with this specific subtype of AML. It has been shown that the patient's age, comorbidity and cytogenetic and molecular abnormalities and thereby subgroup of disease should be considered when deciding treatment, as these factors will have a significant impact on the patient's recovery expectancies (27).

The primary treatment recommended by the Norwegian Directorate of Health and most commonly used for patients up to 65 years is the "7+3"-regimen developed in 1973 (14). The regimen is a combination of infusions of the anthracycline drug daunorubicin (DNR) for 3 days and continuous infusions of the nucleoside metabolic inhibitor cytarabine (ara-C) for 7 days (9). In some cases, idarubicin (IDA) is used as an alternative to DNR (11). Because of the severity of the disease and the rapidness of its development, the cytostatic treatment should be started no longer than five days after diagnosis (11). For patients over 60 years of age, the dosages administered are reduced or palliative care considered if the patient has a poor general condition. This is to minimize drug-related side-effects, including myelosuppression (28). In addition, elderly patients have a high risk of developing complications and comorbidities (29). Thus, there is a dire need for treatments which is tolerable also for the weakest patients, and which also are more efficient to prevent relapse.

An important factor when discussing AML treatment is the frequent relapses followed by treatment resistance. The presence of LSCs surviving the cytostatic treatment eventually leads to relapse and drug resistance for a high number of AML patients (6, 30). Many patients responding well to induction therapy, reaching complete remission, relapses within three years with poor prognosis and few treatment options (10).

The development of alternative treatment options include stem cell transplantations and advanced drug delivery systems (DDSs) (14). Stem cell transplantation is a high-risk procedure that can be offered for patients with high relapse risk to avoid resistance (31). The risks of the operation and graft-versus-host disease associated with the procedure restricts usage to patients under 55-60 years in Norway (32). Liposomal DNR have been tested in the form of Daunoxome to minimize side-effects, but was discontinued as treatment of AML (33). Vyxeos (CPX-351) is a liposomal formulation containing DNR and ara-C in a 1:5 ratio approved for t-AML and AML with myelodysplasia-related changes (AML-MRC) (34). The drug was approved in the USA and the European Union in 2018, and shows a significantly higher overall survival rate than the "7+3"-regime, with less side-effects (17, 34). The liposomal formulation is given

intravenously three times over five days, and is currently undergoing clinical trials for use against other AML subtypes in the USA (35).

1.2. Nanosized drug delivery systems

In the last decades, nanoparticles have been introduced as possible DDSs to overcome difficulties in medical treatment. According to the European commission's definition of nanoparticles, 50% of the total particle population should be in the size distribution of 1-100 nm, but in nanomedicine particles up to 1000 nm in at least one dimension are commonly accepted as nanoparticles (36, 37). Nanoparticles are used in medicine for oral, local, topical and systemic (intravenous) use in the field of anesthetics, iron-replacement therapy, ultrasound enhancement, vaccines, fungal treatment and cancer therapy (28, 38). Figure 1.4 illustrates a selection of established nanotherapeutic platforms. Nanoparticles approved for use in Norway includes Abraxane, albumin-particle bound paclitaxel, used against multiple cancers and SonoVue, a phospholipid stabilized microbubble, used as an ultrasound contrast agent (38-40).

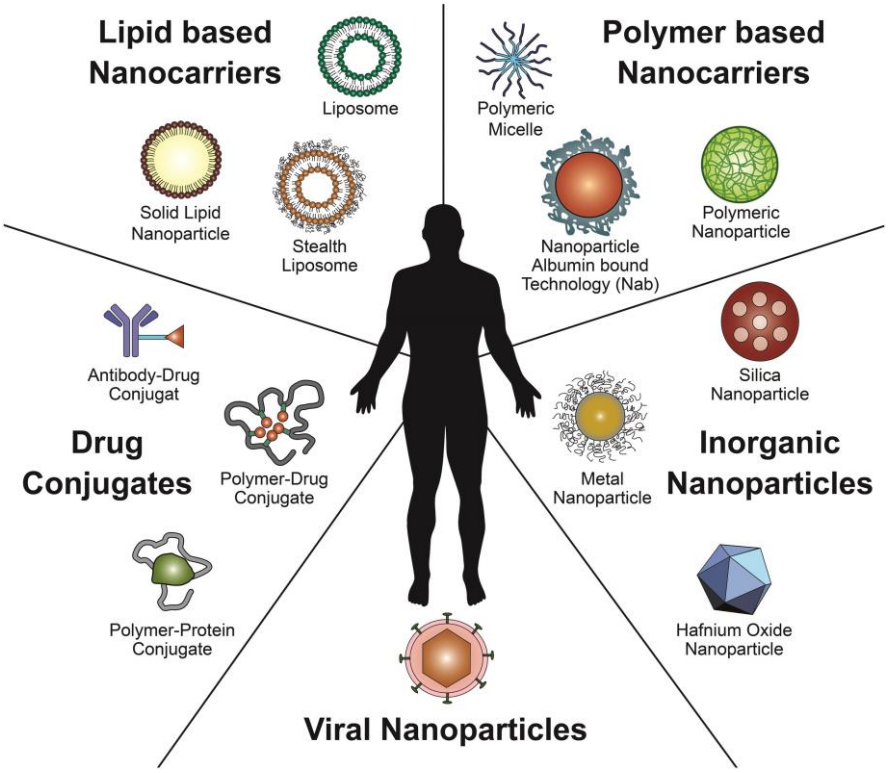

Figure 1.4 - A collection of various nanoparticles in therapeutic use. The figure illustrates nanoparticles produced with different materials, both organic, like lipids, and inorganic, like metal. Figure collected from Wicki, Witzigmann (41).

For simplicity, the term nanocarrier (NC) will be used to describe all nano-sized drug delivery systems. Active ingredients can be encapsulated and protected inside the NCs, like liposomes, or attached on the outside, like for antibody-drug conjugates (38, 41). Advantages of utilizing NCs in drug delivery include the possibilities of targeted drug delivery and stabilizing active substances (42). Chemically unstable drugs or substances with poor water solubility can be encapsulated in NCs, for example liposomes, to improve bioavailability (43). NCs can also be used to ensure that active ingredients reach the drug target at the same time and in an advantageous ratio for drugs composed of multiple substances, for example the liposome Vyxeos (34, 44).

Cytostatics is an example where NCs as a DDS can be advantageous because encapsulation of the toxic compounds can reduce the severe side-effects associated with cytostatic treatment. Cytostatics are often administered in intravenous or oral form, leading to the cytotoxic and cytostatic agents being distributed throughout the body, impacting both healthy and cancerous tissue (41, 43). NCs can minimize the toxic compounds' interaction with healthy tissue, decrease drug resistance and improve targeted distribution. The NC can protect the drug from being prematurely metabolized or eliminated and being engulfed by the immune system (41, 42).

The circulating half-life can be extended by producing the NCs of biocompatible material to avoid triggering an immune response and thus increase the probability of making contact with the target of unhealthy cells (28, 42). Introducing targeting ligands on the NC contributes to it reaching specific receptors expressed on the surface of the cancer cells (14, 45). An example of this is immunoliposomes decorated with monoclonal antibodies binding to antigens on the surface of cancer cells (14). This can prolong the circulation time and therapeutic window by increasing the selective uptake and thereby reducing the needed dosage-effect ratio (37, 41, 42).

Introducing the inert polymer poly(ethylene glycol) $[CH_2CH_2O]_n$ (PEG) on the outsides of NCs will mask them from the immune system, thus avoiding opsonization and further macrophagic phagocytosis (10, 38). PEGylation will also keep the liposomes from agglomerating, as well as extend drug circulation time (46). Agglomeration leads to particles of dissimilar sizes and different drug concentrations, causing it to behave unexpectedly and uncontrollable in the body. Doxil/Caelyx was the first liposomal injection formula containing Doxorubicin (DOX) which utilized PEGylated liposome technology to improve biocompatibility, approved in USA

(33, 38). Studies of the drug showed that the area under the curve (AUC) was increased more than 60-fold compared to free DOX, providing higher probability of the liposomes reaching the target of interest (47). It was also shown that the volume of distribution for the PEGylated NC's is almost identical to the blood volume, indicating that the drug is almost exclusively present in the circulation and very little in the tissue (48). The drug half-life and circulation half-life was increased compared to free DOX (47). A disadvantage of PEGylating liposomes is the association with dose- and frequency related hand-and foot syndrome which is shown to be higher compared to non-PEGylated liposomal formulations (14, 49). However, this might be explained by the PEGylated liposomes circulating longer compared to the non-PEGylated liposomes.

1.2.1. Liposomes

Liposomes are unilamellar vesicles in which an aqueous volume is enclosed by a membrane composed of lipids (50). Figure 1.5 illustrates a liposome where phospholipids with hydrophilic heads and hydrophobic tails form a bilayer. Compared to micelles, which consists of a single layer of lipids forming a hydrophobic core, liposomes will have both hydrophilic and hydrophobic hollows. These properties make them appropriate NCs for transporting both hydrophilic and lipophilic drugs and compounds (51). An example of a phospholipid used to produce liposomes is illustrated in Figure 2.3.

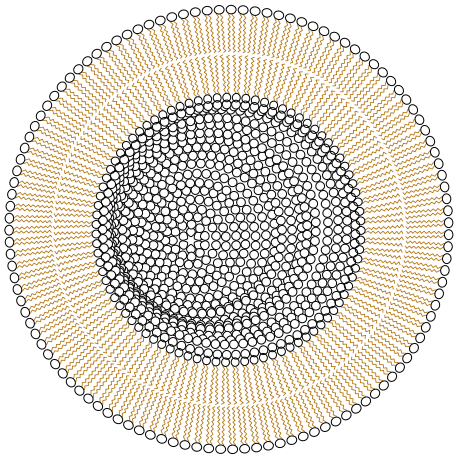

Figure 1.5 - Illustration of a liposome. A cross section of a liposome with the lipid's hydrophobic tails illustrated in light brown forming a lipophilic hollow, and the hydrophilic heads forming an aqueous core. Figure modified from Herfindal, Nilssen (52).

To overcome problems with instability, liposomes can be modified by enclosing cholesterol (Chol) into the membrane (50). Chol will make the membrane more rigid and thereby more stable in terms of leakage. Heat will make the membrane more permeable. By knowing the phase transition temperature, liposomes can be modified to ensure release of an incorporated compound at a desired temperature.

The diameter size of liposomes can vary from tens of nm to several µm (37, 41). For medical purposes, it has been shown that liposomes with diameters around 150-200 nm remain in the bloodstream longer than those with diameters below 70 nm or above 300 nm (53). A compromise must thus be made between increased drug capacity and a higher degree of accurate targeted drug delivery. Generally, smaller liposomes will have reduced drug loading capacity compared to larger liposomes. However, experiments in rodents show that smaller particles evade the bloodstream and penetrate into the tumor interstitium to a higher degree than larger particles. The accumulation of NCs in the tumor interstitium is explained by the enhanced permeability and retention (EPR) effect. (53-56). The EPR effect is the accumulation of molecules inside the tumor because of its pathophysiological properties. The pathophysiological properties within the tumor typically include leaky vasculature and lack of lymph drainage caused by unorganized growing in epithelial tissue (14). However, preliminary studies in the clinic have shown that the EPR effect is tumor dependent and there are substantial individual differences between patients (56).

In earlier research on DNR incorporated into liposomes, the liposomes have been approximately 120-130 nm to secure both an acceptable amount of drug incorporation and enough time spent in the bloodstream (23). The previously mentioned Vyxeos is a non-PEGylated formulation with a liposome size around 100 nm (17). Vyxeos, showing a more positive outcome compared to free DNR and ara-C for t-AML and AML-MRC, gives hope for other liposomal formulations containing DNR to further improve the treatment of AML (17).

1.3. Choice of compounds

Previous research has shown that DNR in combination with a protein synthesis inhibitor (cycloheximide or emetine (EME)) have an increased effect compared to DNR alone (23, 57). Exploiting this synergism can lower the needed dose-effect bar and thereby give fewer dose-related side-effects, such as myelosuppression (58). The synergism has earlier been tested both

as free drugs and incorporated into liposomes and has shown to enhance anthracycline-induced AML cell death *in vitro* and in small animal models (23, 57). Further research has shown that administering EME 30 minutes after DNR would increase the advantageous effect (23). This led Dr. Fabrice Anizon at the University of Clermont Auvergne to formulate an analog of EME, FG1181, shown in Figure 1.7 B. The rationale behind this molecule is that the liposomes will ensure that the two drugs will interact with the blasts at the same time in an optimal ratio. Conversion of FG1181 into EME will ensure that it is active 20-30 minutes after DNR is released. This delayed activation is believed to ensure the desired time difference between DNR and EME. The liposome will protect FG1181 from being metabolized in the blood. Liposomal inclusion of the two compounds would be advantageous as it ensures that both the active substances reach the same target simultaneously. Liposomal incorporation will also ensure equal pharmacokinetics for both compounds, which cannot be achieved if they are administered in separate formulations. Combining the compounds in the same liposomes will also reduce the amount of liposomes needed and thereby decrease the risk of liposomal toxicity such as foot-hand syndrome.

1.3.1. Anthracyclines

Anthracyclines are a class of cytostatic agents with multiple suggested mechanisms of actions (59, 60). The main hypothesis is that anthracyclines intercalate in deoxyribonucleic acid (DNA) and inhibits topoisomerase II, thereby halting mitosis (61). Another effect of anthracyclines is cellular loss of histones, delaying DNR repair in cancer cells (59). Further, anthracyclines generate free radicals which also induce DNA damage as well as damage proteins (62). All the above would affect rapidly dividing malignant cells but also affect several non-malignant cells, leading to the many drug-related side-effects associated with this drug class (6, 61).

The major dose-limiting toxic side-effect of anthracyclines include myelosuppression and cardiotoxicity (14, 58). Especially for DOX, the risk of developing cardiomyopathy and congestive heart failure is increased because of the drug causing severe local tissue necrosis (62). Other drug-related side-effects include alopecia, nauseating and vomiting (63). The risk for cardiotoxicity, myelosuppression, vomiting and alopecia is shown to be significantly lower when incorporating DOX into PEGylated liposomes (63).

The first anthracyclines, DNR and DOX, were isolated in the 1960s and the group has the broadest range of clinical use in oncology compared to other antitumor drugs, with only a few

cancers known to be unresponsive to treatment (58, 60, 64). Figure 1.6 shows the molecular structure of DNR (58). The anthracyclines have fluorescent properties because of its anthraquinone structure, facilitating easy detection in biological samples (65). DOX is still the most commonly used anthracycline in solid tumors, and DNR is generally used against hematological cancers as it currently shows the best results of the available treatment agents available (58).

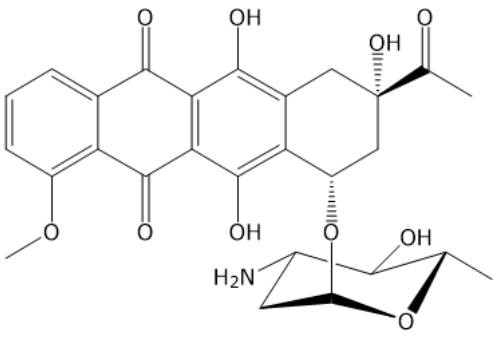

Figure 1.6 – The molecular structure of DNR. The drug is amphiphilic and amphoteric, containing a lipophilic anthracycline ring, hydrophilic hydroxyl groups, an acidic ring phenolic group and basic and lipophilic sugar amino groups (66). Figure adapted from Cortés-Funes and Coronado (58).

Several anthracycline analogs have been developed in the hope of reducing the drug-related side-effects (58). These analogs have some advantages in comparison to the original anthracyclines, but less than anticipated during development. IDA is in some cases used in the "7+3" regime as a replacement for DNR and is the only anthracycline available for oral administration (58). IDA shows a broader spectrum of activity compared to DNR and is used against breast cancer as well as AML, but has the same severe side-effects as DNR (58). Epirubicin is shown to be less cardiotoxic compared to DOX, and shows increased effect against breast cancer in combination with paxitaxel (67).

1.3.2. Emetine and analogs

Emetine (EME) shown in Figure 1.7 A, is a protein synthesis inhibitor derived from the plant ipecac *(Carapichea ipecacuanaha)* and is already approved for use in humans against protozoal infections (68, 69). The compound is a powerful emetic and expectorant, and inhibits the replication of DNA and RNA in viruses (70). EME is highly toxic to all cells and can be modified for use in targeted cancer treatment (71). The compound has relatively equal toxic profile across species, which helps in further investigations and drug development (23). This is an advantage when it comes to cancer therapy because research on cells and small animal models can be translated to cancers in a high degree.

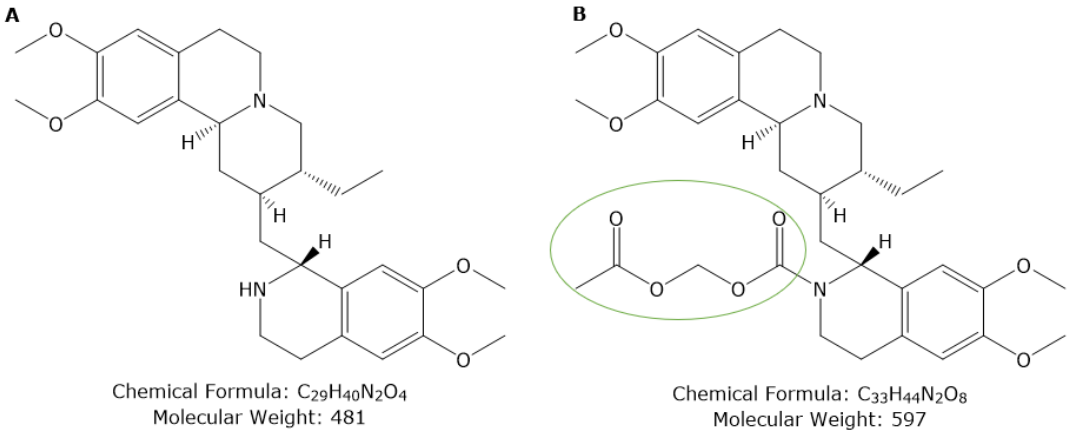

Figure 1.7 – EME and FG1181. Molecular structures**. A,** and **B,** EME and the analog N_2-acetoxymethyl-emetine, termed FG1181. The substituent side chain on the secondary amine is marked in green.

A hypothesis is that exchanging the hydrogen on the N-2' secondary amine of EME with a side chain can lead to an inactivating of the molecule (71). *In vivo* toxicity and anti-cancer activity with EME derivatives were tested with prostate specific antigen activation in 2017, and it was shown that modification with a non-toxic side group can render a non-toxic prodrug with a "cytotoxic switch" (71). The analog N_2-acetoxymethyl-emetine termed FG1181, is shown in Figure 1.7 B. This is a modified version of EME where the hydrogen on the N-2' secondary amine is substituted with a methylene diacetate side chain (green circle in Figure 1.7 B). The hypothesis is that when the side chain is cut off, the molecule will be metabolized to EME and thereby activated. This is estimated to happen 20-30 minutes after the liposome frees the incorporated compound, thus showing improved synergism with DNR compared to EME.

1.4. Aims

The aim of this study was to find an improved treatment method for AML by combining DNR and FG1181 in a liposomal formulation. This can further be divided into three sub-aims.

Firstly, to verify and identify the biological activity of FG1181 and compare its properties to that of EME.

Secondly, to produce a liposomal formulation containing FG1181, both alone and in combination with DNR.

Thirdly, to evaluate the effect of liposomal formulation containing DNR and FG1181 compared to liposomal formulations containing DNR and EME.

2. Experimental theory

2.1. Spectroscopy

Spectroscopy is the study of matter emitting and absorbing radiation, and particles interacting (72). This includes the study of ultraviolet (UV) light, infrared (IR) light, radio waves, x-rays, gamma-rays and visible light, among others (72). Spectroscopy can be utilized to investigate molecular properties such as molecule size and structure, and are used as an analytical method in multiple fields including physics, biology, chemistry etc.

2.1.1. Dynamic light scattering

Dynamic light scattering (DLS) is a technique where the light scattered of a molecule is measured, allowing specific properties of the molecule to be studied (73). The light will interact with particles, where small particles with size ~0.3-10 000 nm (depending on the laser and DLS machine) can be detected as undergoing Brownian motion (74). Brownian motion is the continuous diffusion of a particle when suspended in a fluid as illustrated in Figure 2.1 (75, 76).

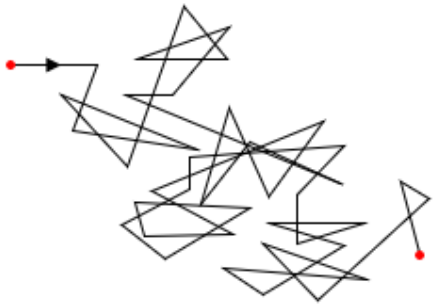

Figure 2.1 - A particle undergoing Brownian motion. The arrow shows which way the particle, marked in red, moves. The apparently random route is termed Brownian motion. Figure adapted from Leybold® (77).

The relationship between the particles' measured Brownian motion can be converted to size and size distribution with the Stokes- Einstein equation shown in Equation 2.1 (78). In the equation, D_T is the diffusion, k_b the Boltzmann constant, T the temperature, η is fluid viscosity and d is the diameter of a sphere with the same speed as the particle (79).

$$D_T = \frac{k_b T}{3\pi\eta d} \qquad \textit{Equation 2.1}$$

The DLS measures diffusion by exposing the sample to a monochromatic wave of light and has photon detectors on all sides measuring light intensity (79). The particles' constant motion will cause a small change in wavelength frequency between unscattered and scattered light, termed a Doppler shift (79). As larger particles move slowly, these will cause a small Doppler shift, while the smaller ones exhibit a larger, more easily detected shift. The light intensity is measured for a period and processed into a mathematical function, identifying patterns where the exponential decay is constant. This gives the diffusion constant, $D_{T,}$ making it possible to calculate the sphere diameter, *d*.(79).

A disadvantage to the DLS is that it measures size indirectly, and that the resulting diameter assumes that the particles are spheres. It also depends on high purity of the samples. Further, if the samples are polydisperse, i.e. that they consist of several size-populations, DLS may not be able to accurately determine individual size-populations, or average size. Therefore, the polydispersity index (PdI), the size population, is given in combination with measurements. However, for routine measurements of liposomes, DLS is a reliable method. Liposomes are spherical, do not interact with the reflected light and the measurements are quick and easily performed.

2.1.2. Infrared spectroscopy

IR spectroscopy measures the absorption of radiation when passing infrared light (700-1000 nm) through a sample (80). An advantage for IR spectroscopy is that it can be used to examine liquids, solids and gases, depending on the instrument and its settings (72). The bonds in molecules and atoms can vibrate in different ways, divided into the subtypes stretching and bending (80). These subtypes can further be subdivided into symmetric and asymmetric stretching, and the bending subtypes into scissoring and rocking. Figure 2.2 illustrates a molecule undergoing symmetric stretching.

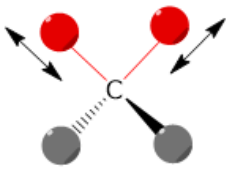

Figure 2.2 - Illustration of a molecule undergoing symmetric stretching. Symmetric stretching of the carbon-hydrogen along the bonds. The red hydrogen atoms stretch to and from the carbon atom at a given frequency making it possible to identify this part of the molecule by IR measuring. Figure adapted from Stuart (80).

As different molecular bonds vibrate with different frequencies, IR measuring can be used to identify the presence of a structure, for example lipids (81). Lipid content can be identified by the vibration of carbon-hydrogen symmetric stretching at ~ 2850 cm^{-1} (80). Figure 2.3 indicates one of the methylene bonds in the phospholipid hydrogenated egg phosphorylcholine (HEPC), making it possible to identify it as a lipid. The resulting peaks at a given energy in an absorption spectrum will correlate to frequencies of a vibrating covalent bond in a molecule (80). IR detection can be used for quantitative analysis as well as for the qualitative analysis described by preparing a calibration curve and comparing the measurements of a sample with unknown concentration.

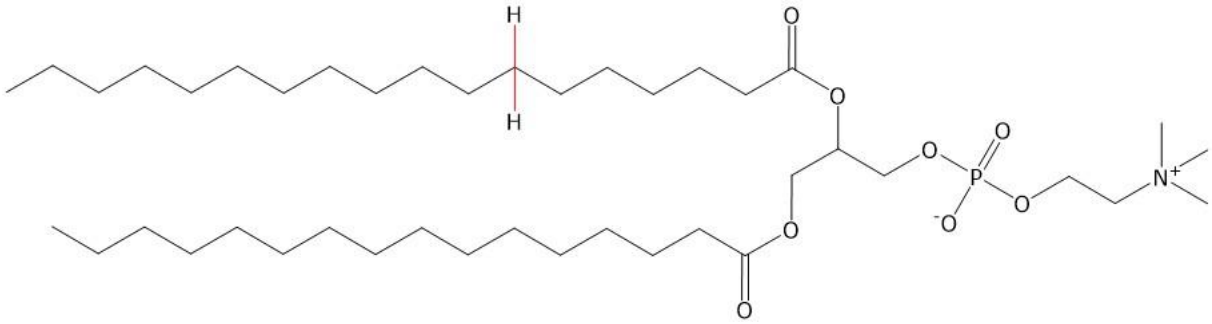

Figure 2.3 - Hydrogenated egg phosphatidylcholine (HEPC). A phospholipid with one of the discussed methylene bonds marked red. Only one out of 34 methylene bonds are marked for simplicity. Figure adapted from Avanti® Polar Lipids (82).

2.2. Western blotting

Western blotting is a technique for detection and quantitation of proteins (83, 84). The technique uses three elements, protein separation by size, transfer of proteins to a solid membrane and target marking with primary and secondary antibody to visualize and quantitate proteins of interest (85). Here, cells were incubated with different compounds, rinses for excess compound, lysating the cells to get all protein in a mixture. The lysate was rinsed from the cell components by centrifugation. To separate by size, the cell lysates, are separated electrophoretically on SDS polyacrylamide gels where an electric force makes the negatively charged proteins migrate (86). Smaller proteins migrate fasten than larger protein, leading to separation.

The protein is further blotted to a polyvindylidene fluorene membrane before being blocked to prevent non-specific binding of applied antibodies. The primary antibody is specific to the protein of interest, and the secondary antibody is specific to the source of the primary antibody. The secondary antibody is often conjugated with an enzyme which will give a signal detectable for the binding. The antibodies will present themselves as bands, where the thickness of the band corresponds to the amount of protein present (85). At last, a loading control is used, for instance anti-β-actin, to control that equal amounts of protein are loaded into each well.

2.3. Chromatography

Chromatography is a collective term for analytical separation (87). The technique is used to separate and purify analytes based on properties like size, charge and hydrophobicity to mention a few (88). The technique is used for quantitative and qualitative analysis by injecting the mixture into a two-phase separating system. One phase is a stable stationary phase, while the other is a mobile phase aiding the analytes through the stationary phase. The mobile phase can be a gas or a liquid. Differences in the properties of the analytes and their interactions with the phases lead to the molecules being eluted separately.

2.3.1. Size exclusion chromatography

Size exclusion chromatography (SEC) separate analytes based on their sizes (89). The technique is also known as gel-filtration chromatography. The stationary phase consists of porous particles, for instance cross-linked dextran polymer gel. Small analytes diffuse into the pores, while larger analytes pass on the outside of the particles (87). The analytes which pass through the porous particles will be retained, and thus elute at a later point compared to the particles that are too large to enter the pores. Figure 2.4 illustrates the process of size exclusion chromatography. A segment of the column is enlarged and a porous particle, encapsulating multiple small and medium analytes in its pores, is shown. The particles will exit the column in order of decreasing size.

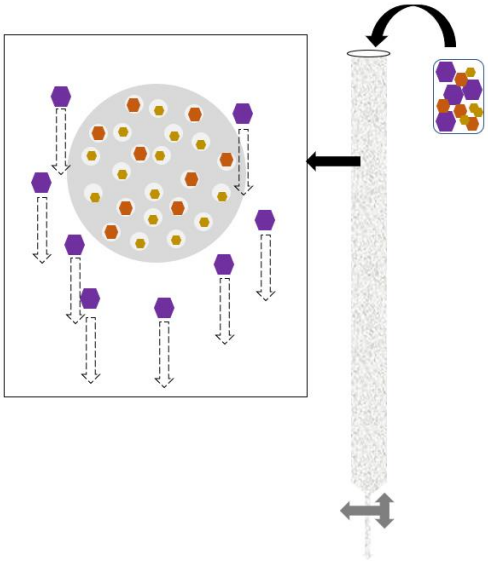

Figure 2.4 - Illustration of Size exclusion chromatography (SEC). A sample containing large (purple), medium (brown) and small (gold) analytes are added to a column with porous particles. The segment shows how the particles encapsulate the smaller and medium analytes while the larger pass on the outside. This happens multiple times throughout the column, causing the delayed elution.

An important consideration when performing SEC is the ability to accurately separate the different particles as they emerge from the column. This can be done by visually inspecting whether the analytes emerging from the column differ in color, or by fractionation. It is also important to choose the right packaging materials because the analytes are separated based on the material's pore size (89). A larger pore size leads to larger analytes diffusing into the pores.

2.3.2. High-performance liquid chromatography

High-performance liquid chromatography (HPLC) is an analytical technique using high pressure to accelerate the process of liquid chromatography (90). The mobile phase is a combination of two or more liquids. The stationary phase is a column consisting of fine particles with diameters ≤ 5 µm (87). The column has higher resolving power if the particles are finer, but this increases the back pressure of the column. These particles form a matrix, which the added sample are eluted through via the mobile phase.

The most common stationary phases are normal and reversed phase, with polar or non-polar stationary phase, respectively (90). The most commonly used method in drug analyses is reverse phase HPLC (RP-HPLC), where non-polar analytes react with the non-polar functional

groups on the stationary phase. RP-HPLC is often used as the mobile phases can consist of simple, inexpensive and safe components, the elution order is easily predicted based on hydrophobicity and the column is reasonably stable (90). Commonly used mobile phases include water, acetonitrile or methanol. The most commonly used reverse phase columns are octadecylsilane (C18) columns. To prolong the life of the main column and prevent the column from clogging, a guard column can be used (90). The guard column should have a small internal volume to minimize peak broadening.

Ultraviolet (UV) light is emitted through the detector, and as the UV radiation is absorbed by the sample components, the detector observes a reduced signal (90). The UV detector can be set to measure at a fixed wavelength, at variable wavelengths or with a diode array that measures a spectrum of wavelengths simultaneously. The resulting peaks can be further analyzed as wanted.

2.4. Membrane permeability

The parallel artificial membrane permeability assay (PAMPA) is a model for measuring passive diffusion across a membrane (91). An artificial membrane can be used to characterize a compound's ability to passively diffuse across physiological membranes, for instance the blood-brain barrier or liposomal membranes (92). This is an important part of drug delivery development, because some drugs, for instance Daunorubicin (DNR), is known to be a substrate for active transport over membranes (93). This means that for DNR to cross the liposomal membrane, the temperature must exceed the phase transition temperature.

Membranes for PAMPA can be purchased premade or be individually adapted to a specific assay by adding cholesterol. A setup can for instance consist of a plate with 96 wells with membranes of 0.45 µm pores made of Polyvinylidene fluoride (94). The bottom plate consists of donor wells filled with samples diluted in buffer. The top plate is placed onto the bottom plate. The top plate has a semipermeable membrane in the bottom of each well, which each are filled with buffer solution. The drugs can passively diffuse through the membrane into the acceptor wells, but not back to the donor wells. This is indicated by the one-sided arrows in Figure 2.6 which illustrates a well in a PAMPA plate. After 4-5 hours of incubation, acceptor and donor wells are analyzed to find effective permeability, $\log(P_{eff})$. A definition gives measured $\log(P_{eff}) < -6.14$ as impermeable, $-6.14 < \log(P_{eff}) < -5.66$ as low permeability and -

5.66 < log(P_{eff}) < -5.33 as intermediate permeability (95). Log(P_{eff}) over < -5.33 are considered as highly permeable. An advantage when performing PAMPA is that it is easy, but it is important to consider the shortcomings- including the possibility of incorrect predictions and reproducibility difficulties (91).

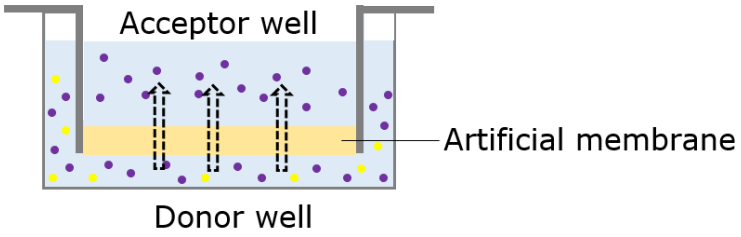

Figure 2.6 - Well in PAMPA-plate. The small purple particles indicate a drug able to diffuse through the membrane, while the yellow particles are a drug which cannot passively diffuse through the membrane. Figure adapted from Creative Bioarray (96).

2.5. Assessment of cellular cytotoxicity

In vitro assessments are necessary to carry out before conducting *in vivo* trials, but it is important to note that these will give different results. *In vivo* assays are more controlled, not including factors like the human immune systems. The use of knockout mice as models for cancer, for instance, does not take into consideration the fact that germline mutations often lead to embryonic or early postnatal death (97). Some cancers in humans are triggered by a somatic mutation leading to a centered tumor growth, while whole-body gene knockout mice can have the mutation in every gene. The *in vitro* assessments give valuable information regarding further development, but the results must be critically reviewed before concluding that the results apply for human cancers.

2.5.1. Cell lines

The use of cell lines for *in vitro* cell assessments gives the opportunity to test a compound on a specific cell type. However, the effect on healthy cells and the immune system's response is not measured when testing a cytotoxic compound on a malignant cell line. Chemotherapy is known to damage the host immune cells, leaving the immune system impaired to fight remaining cancer cells and inhibit tumor growth (98).

The cell lines used in this study includes malignant and non- malignant cells, with a focus on the monocytic leukemia cell line MOLM13 (ACC, 554) (99). MOLM13 was collected from a human 20-year old male diagnosed with the AML subtype FAB M5a after relapse in 1995 (100). The non-malignant cell lines NRK (ATCC, CRL-6509) and H9c2 (ATCC, CRL-1446) were used as non-malignant comparisons (99). NRK cells are rat kidney fibroblast cells (101). H9c2 cells are rat heart/myocardium myoblast cells (102). The non-malignant cell lines can be used to estimate a compound's effect on non-mutated human cells and thereby drug-related side-effect.

2.5.2. Assessment of cell viability

Cell viability can be estimated using metabolic activity indicators. An example of this is performing colorimetric assays utilizing water soluble tetrazolium salt-1 (WST-1) as a proliferation agent (103). A colorimetric assay determined the metabolic activity in a sample by comparing the colored substances relative to control (104). The stable tetrazolium salt WST-1 is cleaved enzymatically by NAD(P)H (noted as EC in Figure 2.5) reductase to a soluble formazan dye as shown in Figure 2.5. The formazan has a dark red color, thus making it possible to use a spectrophotometer to measure absorbance. The amount of formazan dye formed directly correlate to the number of metabolically active cells in cell culture, making it possible to estimate metabolic activity relative to untreated control cells (103).

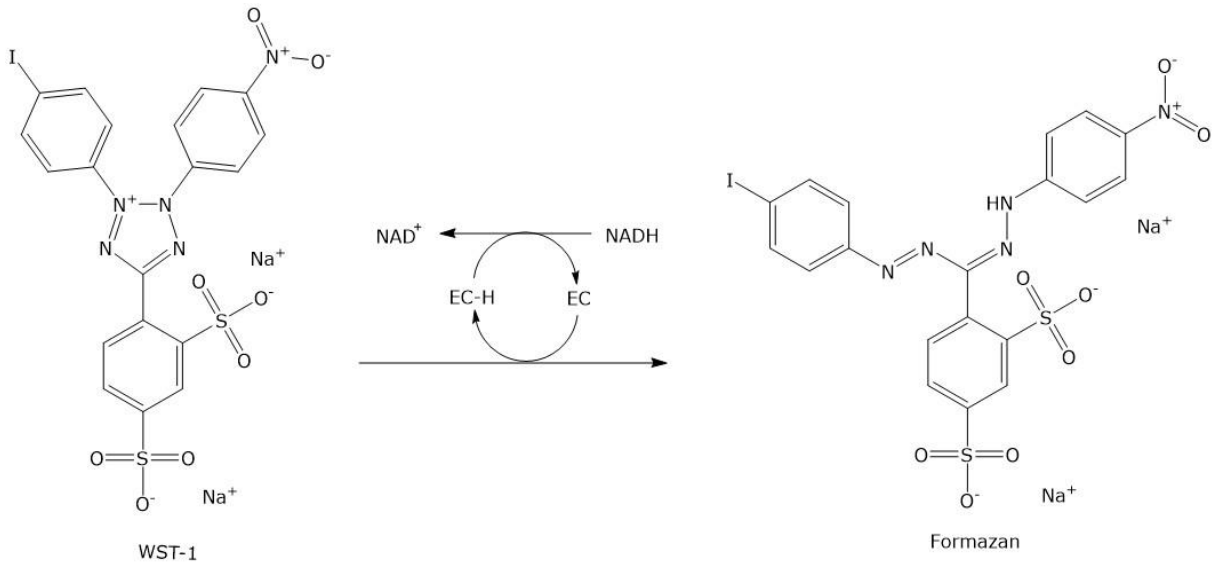

Figure 2.5 - Illustration of a cell proliferation reagent reaction. WST-1 is being reduced to Formazan. The WST-1 reagent has a slightly red color, while the Formazan is dark red. Formazan enters the nucleus, coloring it red. Figure adapted from product sheet at Merck (103).

A disadvantage of using the WST-1 colorimetric assay is that substances of strong (red) colored compounds can influence the spectrophotometer by giving a higher reading for metabolic activity. This makes it necessary to visually check the wells to ensure correct results. A fluorescence microscope can be used if the cells are stained with a fluorescent stain, for instance Hoechst 33342 which will color DNA blue (105). However, visually confirming if cells are normal or apoptotic can be difficult to accurately quantify. Combining the two methods of finding a ratio for living/dead cells can be combined to find an acceptable result.

3. Materials and methods

3.1 Materials and reagents

FG1181 precured from Dr. Fabrice Anizon (University of Clermont Auvergne, France).

1,2-Disteraoyl-sn-glycero-3-Phosphoetanolamine-N- [Methoxy(Polyethylene glycol)-2000] (ammonium salt) (DSPE-PEG), Whatman® Nucleopore Track- Etched membrane filters and 1,2-distearoyl-sn-glycero-3-phosphoethanolamine-N-[folate(polyethylene glycol)-5000] (ammonium salt) (DPSE-PEG(5000)folate) from Avanti ® Polar Lipids (Alabaster, AL, USA).

Quick Start™ Bradford 1x Dye Reagent (12% 10 well), 50 µL/well Mini-Protean® TGX™ Precast Gels, Precision Plus Protein Standard, immune-Blot® PVDF Membranes for Protein Blotting, 10x Tris/Glycine (TG) buffer and 10x Tris/Glycine/SDS (TGS) buffer from Bio-rad (Hercules, CA, USA).

Corning® Gentest™ Pre-coated PAMPA Plate system from Corning® (Corning, NY, USA).

Chloroform and Dimethyl sulfoxide (DMSO) ≥ 99.5% from Honeywell chemicals (Morris Plains, NJ, USA).

Hydrogenated egg phosphatidylcholine (HEPC) from Lipoid GmbH (Ludwigshafen, Germany).

Sephadex™ G-50, ≥ 99.5% sodium chloride, cholesterol (Chol), ammonium sulphat, phosphate buffered saline (PBS), hydrochloric acid, sodium hydroxide, emetine (EME), trifluoroacetic acid (TFA), 37% formaldehyde, 0.01 mg/mL Hoechst 33342, RPMI medium, Dulbecco's modified Eagle's medium (DMEM), Penicillin, Streptomycin. L-Glutamine solution (L-glut), fetal bovine serum (FBS), Tween ® 20, ≥ 99.9% Trizma ® base (TBS), ≥ 99.8% methanol, Ponceau S solution, Bromophenol Blue sodium salt, NP-40%, EDTA, DTT, NaF, MgCl2*6H2O, 86-89% glycerol solution, ≥ 99.9% Acetonitrile (ACN) and ≥ 99.9% Methanol for HPLC from Merck (Darmstadt, Germany). *Earlier Sigma/ Sigma-Aldrich (St. Louis, MO, USA).

WST-1 Cell Proliferation Assay Reagent and cOmplete tablets, Mini EDTA-free EASYpack, protease Inhibitor Cocktail Tablets from Roche Applied Science (Penzberg, Germany).

UltraCruz® suspension culture bottles with vent cap from Santa Cruz Biotechnology, Inc. (Dallas, TX, USA).

DNR (Cerubidine) from Sanofi Aventis (Lysaker, Norway).

96-MicroWell™ plates with flat bottoms, Nunc™ 12-well multidishes, Pierce™ Bovine Serum Albumin Standard, Tropix® I-block™, SuperSignal® West Pico Chemiluminescent Substrate and West Pico PLUS chemiluminescent Substrate from Thermo Scientific (Waltham, MA, USA).

3.2 Equipment and instrumentation

DLS was measured with a Zetasizer Nano XS from Malvern Panalytical (Almelo, Netherland). The IR spectroscopy was performed with Direct Detect Assay-free Cards on a Direct Detect ® Spectrometer from Merck Millipore (Darmstadt, Germany). SEC was performed with an Econo- Column from BioRad (Hercules, CA, USA). Extrusion was performed with a mini extruder from Avanti ® Polar Lipids (Alabaster, AL, USA) and a LIPEX™ gas extruder from Northern Lipids (Burnaby, Canada). The fluorescence microscope used was a Diaphot 300 Inverted Microsope from Nikon (Minato, Tokyo, Japan).

HPLC was performed with a Merck-Hitachi LaChrome HPLC machine from VWR (WestChester, USA), consisting of a Merck L-7614 pump, a Rheodyne® 7725i manual injector, 250 µL 1725N syringe from Gastight® from Merck*(Darmstadt, Germany), a Kromasil 100-5C18 150-4.6 mm reverse phase column (Akzo Nobel, Sweden), a L-7455 diode array detector, Hitachi Interface D-7000 and the data processing software D-7000 HPLC system Manager (HSM) version 4.1. *Earlier Sigma/ Sigma-Aldrich (St. Louis, MO, USA)

The thermomixer comfort was from Eppendorf AG (Hamburg, Germany), the Zentrifugen universal 32 centrifuge from Hettich (Tuttlingen, Germany), the humidified Steri-Cycle CO_2 incubator from Thermo Scientific (Waltham, MA, USA), the Olympus CKX31 microscope (Shinjuku, Tokyo, Japan), 2103 Envision Multilabel Plate Reader from PerkinElmer(Waltham, MA, USA), the Allegra™ X-22R Centrifuge from Beckman Coulter (Brea, CA, USA), the ImageQuant LAS 4000 camera system from GE Healthcare (Chicago, IL, USA) utilizing the program “Image Quant LAS400”, the Mini-Protean® Tetra system blotting chambers from

BioRad (Hercules, CA, USA) and the Scanlaf Laminar Air Flow (LAF) Mars safety benches from Labogene (Allerød, Denmark).

3.3 Production of liposomes

3.3.1 Preparation of liposomes

HEPC, Chol and DSPE-PEG were dissolved in chloroform at concentrations of 2.37 mg/mL HEPC, 0.65 mg/mL Chol, and 0.71 mg/mL PEG-PE. Ten mL from each of the stock solutions were mixed in a 200 mL round bottom flask, giving a molar ratio of 1.81 HEPC: 1 cholesterol: 0.15 DSPE-PEG. For the production of folate decorated liposomes, DSPE-PEG(5000)folate was added at one tenth of the molar concentration of DSPE-PEG by adding 10 mL 0.16 mg/mL DSPE-PEG(5000)folate dissolved in chloroform to the round bottom flask in addition to the other lipids.

A lipid film was produced by evaporation of the chloroform using a rotary evaporator at 200 mbar and 60 RPM for 60-90 minutes without heating and then at 20℃ using a water bath until the film appeared dry. Residual chloroform was removed by running the vacuum pump at maximum pump capacity (7-8 mbar) for 30 minutes. The film was hydrated with 10 mL 250 mM ammonium sulphate adjusted to pH 6-6.5 and heated to 60-65℃. To completely hydrate the lipid film, it was thoroughly vortexed at 60℃ until no lipid film was visible on the round bottomed flask. This produced large multilamellar vesicles (LMV) which were further extruded to produce small unilamellar vesicles, also called liposomes.

Extrusion was performed by using a mini syringe-extruder for small volumes, or a gas extruder for large volumes. For the mini extruder, the LMV suspension were passed through 19 mm Φ membrane filters with decreasing pore size. The suspension was passed 11 times through 400 nm filters, 11 times through 200 nm filters and finally 22 times through 100 nm filters. The gas extrusion was performed with 25 mm Φ membrane filters 5 times through 800 nm filters, 5 times through 400 nm filters, 10 times through 200 nm filters and 10 times through 100 nm filters. This ensured liposomes with diameter of approximately 115-135 nm and acceptable polydispersity index (PdI), measured with DLS (see experimental theory section, chapter 2.1.1).

SEC with degassed PBS adjusted to pH 8.0 was performed to change the buffer around the liposomes (see experimental theory section, chapter 2.3.1). If the column was left unused for more than a month, empty liposomes were sent through before use. The liposomal formulation was stored at 4℃ in the dark for up to nine days before being used in experiments and shaken vigorously before every use. The lipid content was measured using IR spectroscopy and calculated using a previously obtained standard curve with equation 3.1 where *y* are the readings from the IR spectroscope, and *x* the lipid concentration in mg/mL (see experimental theory section, chapter 2.1.2) (106).

$$Standard\ curve: y = 0.0147x \qquad Equation\ 3.1$$

3.3.2 Compound loading of liposomes

FG1181 was dissolved in DMSO, DNR and EME were dissolved in PBS. The liposomes were loaded with 1:10 DNR: lipid solution and/or 1:5 or 1:10 EME or FG1181 compound/lipid content by two methods, either leaving the solution in the dark at 4℃ overnight or under stirring for one hour at 60℃. After loading, the liposomes went through SEC to remove non-encapsulated compound, the lipid contents were measured with IR and the sizes measured with DLS.

3.3.3 Reverse phase high performance liquid chromatography

Reverse phase high performance liquid chromatography (RP- HPLC) was used to separate and quantify the compounds in the liposomal formulations with equipment specified in the equipment and instrumentation chapter 3.2. Ten µL samples were loaded onto the column. The samples used were dissolved in 30% ACN and MilliQ (MQ). Two set ups for mobile phase composition and gradients were used. The gradients of the components are plotted in Figure 3.1. The first mobile composition, A1 and B, were A1: 2:8 MeOH:MQ added 0.05% and B: ACN added 0.005% TFA. The second, A2 and B, were MQ added 0.05% TFA and B ACN added 0.005% TFA. Spectra from 190-550 nm were recorded every 0.2 sec, and integration of peaks was on chromatogram created at 280 nm.

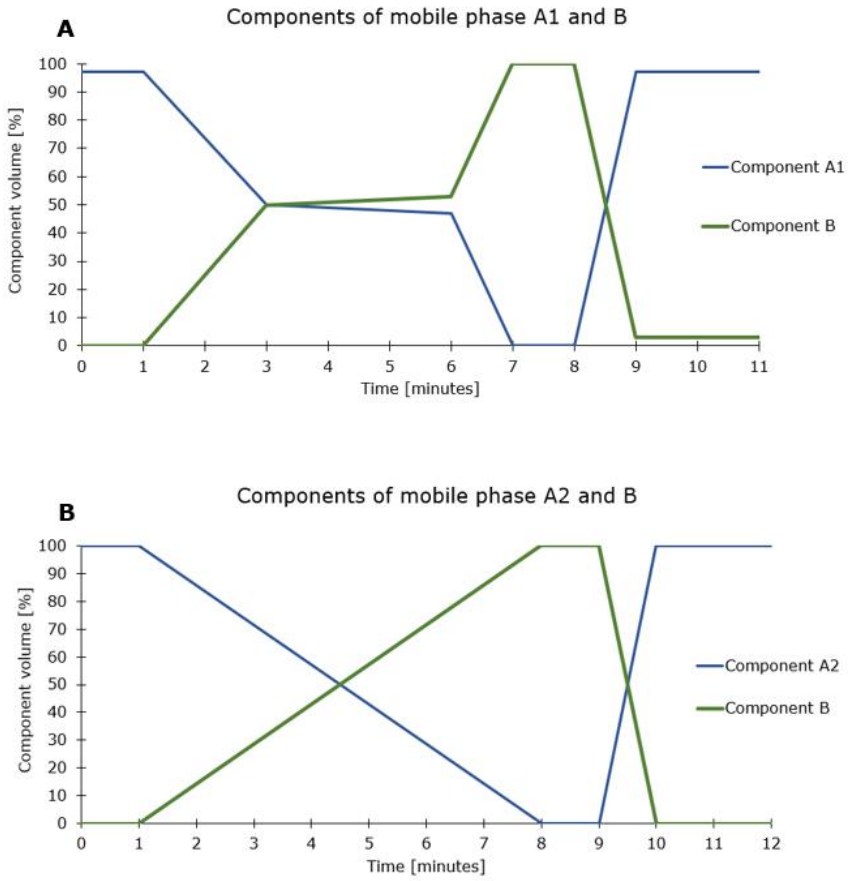

Figure 3.1 – Mobile phase gradients. Scheme of the percentage of each component in the mobile phases. Note that the gradients extend over different time periods.

3.4 Parallel artificial membrane permeability assay

Parallel artificial membrane permeability assay (PAMPA) was performed to estimate if and to which extent FG1181 and EME passively cross over a phospholipid membrane. The assay was performed according to the manufacturer's instructions. In brief, the compounds were dissolved to 50 µM in buffer, and added to the donor wells. The membrane plate was added, and buffer added to the acceptor wells. The buffers were PBS pH 7.4 or pH 8.0 in the donor wells and PBS pH 7.4 or 250 mm ammonium sulphate pH 6.4 in the acceptor wells. This would mimic the pH conditions during compound loading of liposomes. After assembly of the plate, it was left in the dark at room temperature for 5 hours before the constituents of the donor and acceptor wells were collected and the compound content analyzed by HPLC as described in section 3.3.3. The compounds were tested both alone and in combination under the different pH conditions. The ratio between drug in the acceptor wells and donor wells were calculated.

The effective permeability, P_{eff}, [cm/s] was calculated using Equation 3.3, where A is the area of the filter plate membrane, V_D and V_A are the volumes of the donor and acceptor wells, $C_A(t)$ is the concentration in the acceptor well at time t, and t is the time of incubations (107). C_{eq} was calculated using Equation 3.4, where $C_D(t)$ is the concentration in donor well at time t.

$$P_{eff} = \frac{-\ln\left(1-\frac{C_A(t)}{C_{eq}}\right)}{A\cdot\left(\frac{1}{V_D}+\frac{1}{V_A}\right)\cdot t} \qquad \textit{Equation 3.3}$$

$$C_{eq} = \frac{(C_D(t)\cdot V_D + C_A(t)\cdot V_A)}{(V_D+V_A)} \qquad \textit{Equation 3.4}$$

3.5 Cell maintenance and experiments

3.5.1 Cell maintenance

The MOLM13 cell line are suspension cells which were cultured in RPMI-1640 growth medium, enriched with 100 IU/mL penicillin, 100 mg/L streptomycin, 0.2 mM L-Glut and 10% FBS. NRK and H9c2 are adherent cell lines which were cultured in Dulbecco's modified Eagle's medium (DMEM), enriched with 100 IU/mL penicillin, 100 mg/L streptomycin and 10% FBS. The cells were incubated at 37℃ in the dark with 5% CO_2 in the air. The H9c2 and NRK were detached from the incubation flask by washing twice with room temperature PBS and incubating with 0.33 mg/mL trypsin for 2-3 minutes at 37℃. To resuspend all the cell lines, the cells were centrifuged at 200xG for 3 minutes and the cell pellet reseeded in fresh medium. All cell handling was performed in a LAF bench and inspected in a microscope.

3.5.2 Metabolic activity measurements

Dose-response assays were performed with 100 µL medium as blanks, and 50 µL medium and 50 µL cells of approximately 400 000 cells/mL as control. Ten µL drug or 20 µL liposomal solutions were mixed in 80 µL medium before being sequentially diluted in 50 µL medium across the plate. 50 µL cells were added to all wells except the blanks. All parallels were carried out in triplets, including blanks and controls. The wells on the edges of microplates were not used for cells but filled with sterile liquid to avoid edge effect due to for instance liquid evaporation. 96-well microplates were used to carry out all cell assays. The plates were

incubated at 37℃, 5% CO_2 for 22-24 hours. Ten µL WST-1 Cell Proliferation Reagent was added to each well and the plate was further incubated for two hours (see chapter 2.5.2). The plate was then analyzed using a spectrophotometer measuring absorbance at 450 nm, with a reference read at 620 nm. The measurements were adjusted relative to blanc and control with Equation 3.5.

$$Metabolic\ activity = \frac{m_{sample}}{m_{blank}} - m_{control} \qquad Equation\ 3.5$$

To visualize the nuclei of the cells, 100 µL 4% Fix, consisting of 4% formaldehyde and 0.01 mg/mL Hoechst 33342 in PBS pH 7.4, was added to each well. Images were obtained using a fluorescence microscope fitted with a camera and the percent of apoptotic, necrotic and normal nuclei determined. The pictures were imported to ImageJ to calculate mortality depending on drug concentration.

3.5.3 Kinetics assay

To assess the induction of apoptosis over time, compounds were added to cells, and aliquots transferred to 2% formaldehyde in PBS pH 7.4, added 0.01 mg/mL Hoechst 33342 at different time-points for 24 hours. To compensate for cell death in the control, the data was adjusted with Equation 3.6.

$$Adjusted\ sample\ =\ sample\ -\left(control\ \cdot\ \frac{100\ -sample}{100\ -control}\right) \quad Equation\ 3.6$$

3.6 Protein detection

After one-hour treatment at 37℃ with compounds, MOLM13 AML cells were rinsed twice with 4℃ 9 mg/mL NaCl by centrifugation at 1200 RPM for 5 minutes at 4℃. The cells were then lysed in 100 µL SHIEH-buffer consisting of 10 mM Tris HCl pH 7.5, 1 mM EDTA, 40 mM natrium chloride, 10% glycerol, 0.5 % NP-40, 5 mM sodium fluoride, 0.5 mM sodium orthovanadate and 1 mM DTT in MQ. The lysis was performed by incubation on ice for 30 minutes before being centrifuged at 13 000 RPM for 30 minutes at 4℃.

To determine the protein concentration of the lysate, a standard curve of Bovine Serum Albumin Standard and dye reagent were prepared with concentrations of 0, 2, 4, 6, 8 and 10 mg/mL according to the manufacturer's instructions. 2 µL lysate from each sample (described in Section 3.9.1) were dissolved in 998 µL dye reagent in Eppendorf tubes. Triplets of 200 µL standard curve and samples were prepared on a 96-well microplate and left for more than five minutes. The plate was introduced into a spectrophotometer reading at 595 nm, and the protein concentration calculated from the equation obtained from the standard curve.

Before SDS-PAGE, 50 µL samples containing 1 mg/mL protein were prepared in 10% 5x loading buffer, consisting of 1% SDS solution, 12 mM Tris-HCl pH 6.8, 0.1% Bromophenol Blue, 50mM DTT and 10% glycerol in MQ, and 1 x protease synthesis inhibitor in SHIEH-buffer. The samples were heated for 10 minutes at 100℃, before being left on ice for 20 minutes. Twenty µL of the standard Precision Plus Protein Standard All Blue was added to the second well, while the outermost wells were left open. Forty µL sample were introduced in every well of a 12% precast gel for 90 minutes on 100 V in an SDS-PAGE chamber with TGS as running buffer to transfer the proteins to a polyvinylidene fluoride membrane. The blotting was left running for 70 minutes in a blotting chamber at 100 V using a blotting buffer consisting of 10% MeOH and 10% TG in MQ. The membrane was thoroughly washed three times in TBS-T consisting of 1% TBS and 1% Tween in MQ.

Ponceau S solution was added to the membrane and the excessive solution washed away with MQ to ensure the presence of protein bands. The membrane was photographed (Appendix I) before all the Ponceau S solution were rinsed away with 0.1 M Sodium hydroxide and MQ. The membrane was thoroughly washed three times in TBS-T.

The blocking buffer was produced by adding 2.0 g I-Block powder in 1L TBS heat to 70℃, cool down to 20℃, add 2.18 g MgCl2*6H2O and 1 mL Tween. The membrane was blocked for 60 minutes on a shaker before being washed thoroughly with TBS-T three times. Five mL caspase-3 mouse monoclonal IgG_{2a} from Santa Cruz Biotechnology (Dallas, TX, USA) was incubated with the membrane on rotation in the dark at 4℃ for 18 hours overnight (108). The next day, the membrane was thoroughly rinsed again with TBS-T, before incubation with the secondary antibody, donkey anti-mouse horseradish peroxidase (AB2340770, product nr. 711-035-150) from Jackson ImmunoResearch Europe Ltd (Cambridgeshire, UK) for 60 minutes on rotation in room temperature. The antibody solution was removed and washed again with TBS-T. 2 mL chemiluminescent substrate (SuperSignal™) was applied to the membrane for 3.5

minutes and a picture taken with a chemiluminescence and fluorescence digital imaging system for gels and blots. The (Appendix I).

The TBS-T rinsing step was repeated, and the membrane left in mouse anti-β-actin antibody (AC-15 (ab6276)) from Abcam (Cambridge, UK) for one hour. The β-actin was removed, and the membrane rinsed with TBS-T. 2 mL chemiluminescent substrate (West Pico Plus) was added for one minute, and a new picture taken (Appendix I).

3.7 *In silico* prediction, data analysis and presentation

In silico prediction was performed by drawing the structures in ChemDraw Professional version 16.0 (PerkinElmer Informatics Inc. Waltham, MA, USA) and using the net charge prediction plug-in Marvin Sketch version 19.1 (ChemAxon Ltd., Budapest, Hungary). Fluorescent images were analyzed with NIH Image J version 1.52a. All data are presented as averages with standard deviation ($n \geq 3$). The data was processed using Microsoft Office Excel version 16.0.

4 Results

4.1 FG1181 chemical properties and anti-AML activity

Before starting the work with loading the emetine analog FG1181 into liposomes, we needed to perform characterization of the chemical properties of the compound, as well as its cytotoxic potential. This, to ensure that the compound was a valid drug candidate for AML therapy. *In silico* predictions of net charge as a function of pH could give an indication of the ability of FG1181 to cross membranes. These showed that the protonated form was the dominating specie below pH 8.5, whereas the molecule became fully uncharged above pH 10.0. Note that while EME has a net charge of +2 at acidic conditions, FG1181 only has +1 due to the hydrogen being substituted at EME's secondary amine (green circle in Figure 4.1 A). DNR is negatively charged above pH 9.0, and positively charged at pH below 8.5, but there is a pH window between 8.0 and 10.0 where the dominating specie of all molecules will be uncharged. This suggests that the same conditions for post-loading of liposomes could be used for FG1181 as was described for EME and DNR (23).

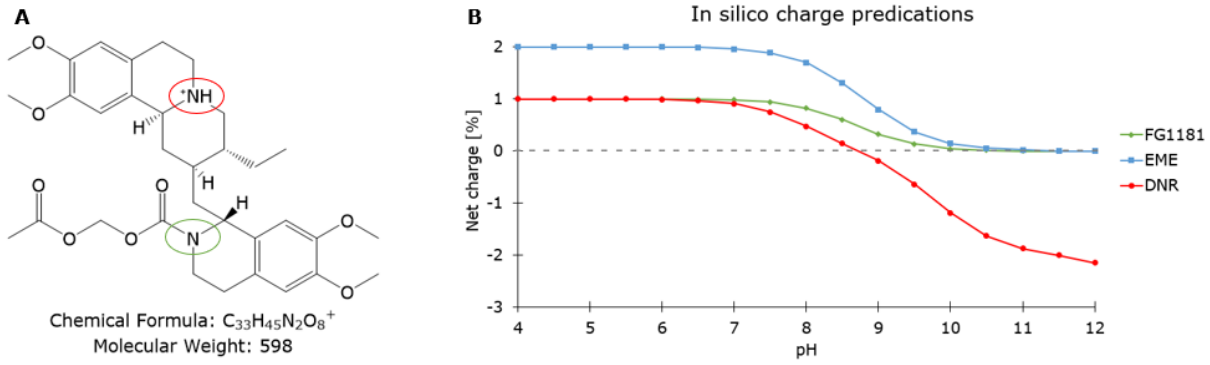

Figure 4.1 – Net charge predictions of FG1181. A, The estimated molecular form of protonated FG1181 with the affected amine and added proton encircled red. The protonation leads to the compound getting a net charge of +1. The other nitrogen, marked green, indicates the amine where the substituent is attached on EME to produce FG1181. Emetine (EME) can be protonated at both the encircled nitrogens, giving a net charge of +2. **B,** *In silico* net charge predictions for FG1181, EME and Daunorubicin (DNR), made using Marvin Sketch.

Next, we wanted to verify the findings from the *in silico* prediction by using PAMPA. Here the drug content of the donor and acceptor wells are measured by RP-HPLC, and two sets of standard curves for DNR, EME and FG1181 were prepared to be able to quantify the

compounds. This was done with different mobile phase composition and gradients, as described in the Method section, chapter 3.3.3. The second set of standard curves with equations from linear regressions are presented in Figure 4.2.

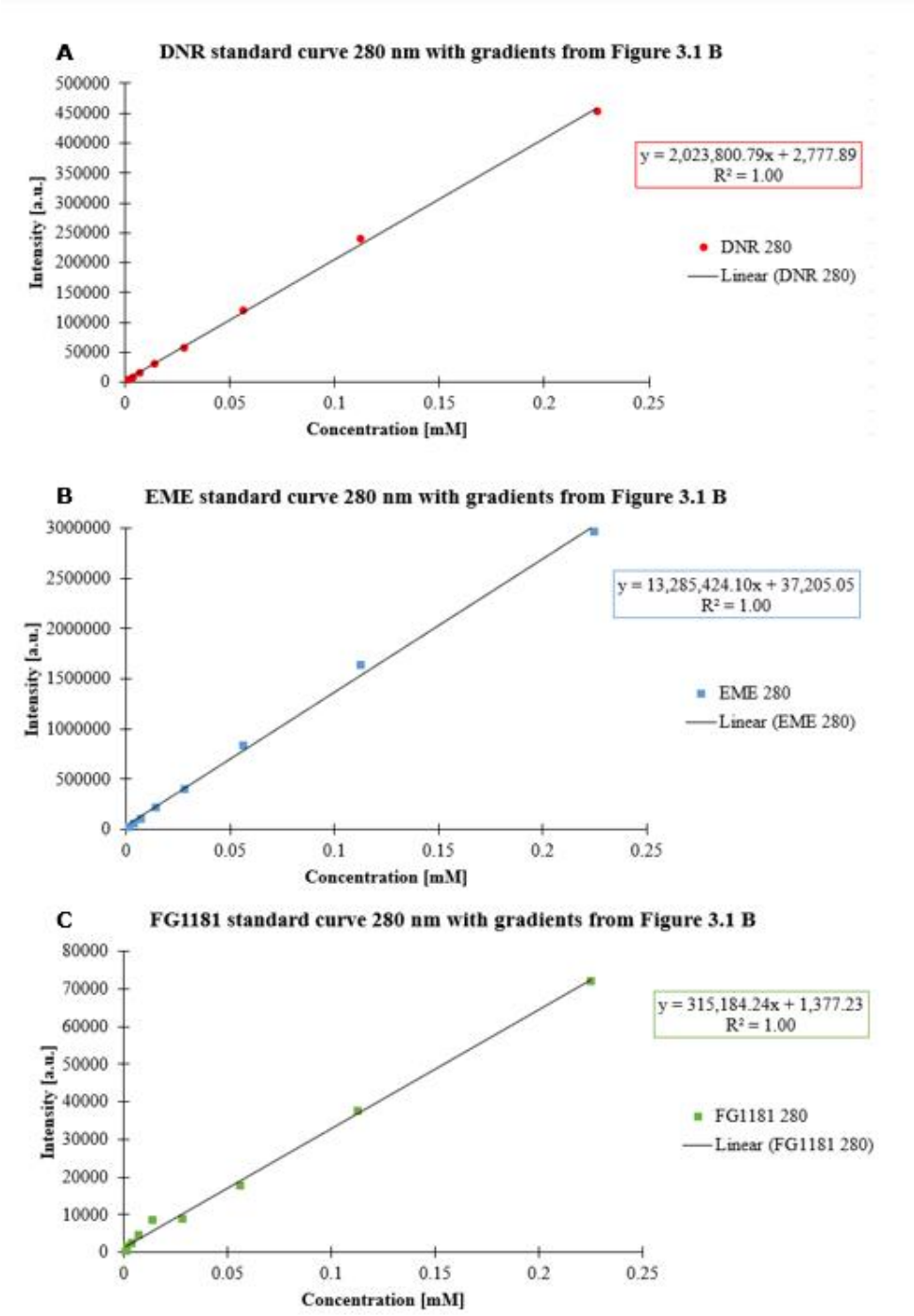

Figure 4.2 – Standard curves produced with RP-HPLC. A-C, Standard curves for Daunorubicin (DNR), emetine (EME) and FG1181, respectively. The given equations were used to calculate compound concentration in PAMPA and in compound-loaded liposomes. The standard curves were produced as described in Section 3.3.3 and Figure 3.1 B.

PAMPA was performed to estimate the different compounds' ability to cross the liposomal membrane. In the assay, two different pH conditions were examined. Examples of RP-HPLC spectra are shown in Figure 4.3 and the results presented in Figure 4.4 and Figure 4.5. Note that in all the FG1181 donor wells, an extra peak at approximately t ~ 5.60 was detected in the spectrums. This is marked with a black arrow in Figure 4.3 and as "FG1181*" in Figure 4.4. Note that more compound passes the membrane for pH 8.0 in the acceptor wells and 6.4 in the donor wells compared to pH 7.4 in both wells. This is particularly evident for FG1181, but there is also an increased proportion of DNR and EME in the acceptor wells. In line with this, we observed increased permeability (log(P_{eff})) with pH 8.0 in the donor wells, and 6.4 in the acceptor wells compared to pH 7.4 in both wells, as illustrated in Figure 4.5.

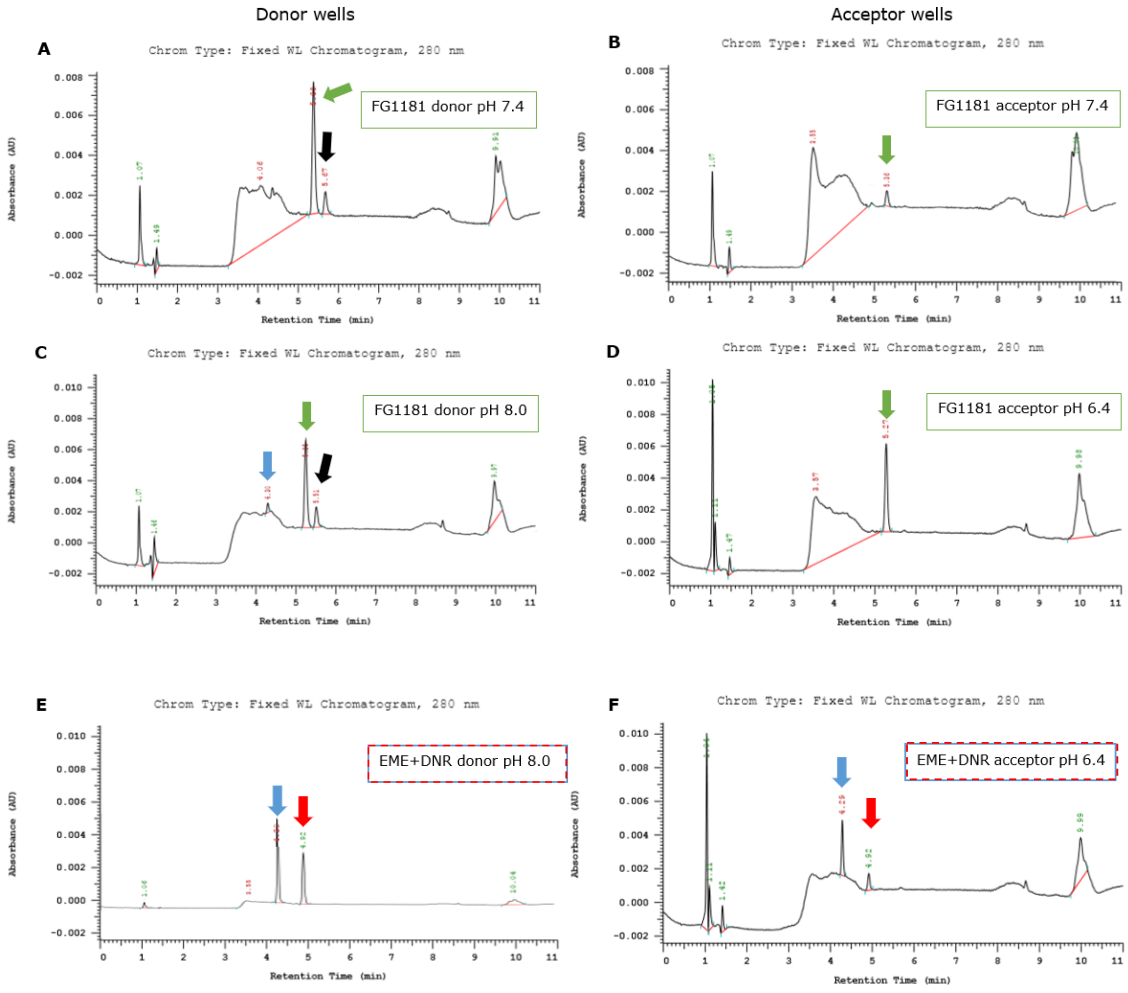

Figure 4.3 – RP-HPLC spectra of FG1181, emetine (EME) and daunorubicin (DNR) from the PAMPA samples. One experiment in the PAMPA with examples of spectra detected from different wells. The arrows indicate the different compounds, with FG1181, EME and DNR marked as green, blue and red, respectively. The black arrows indicate the product noted as FG1181* in Figure 4.4. See respective figures for specification of well and pH- condition. Note that the values for the x-axes in **A** and **B** is lower than for **C-F**. For details on the HPLC set-up and PAMPA, see chapters 3.3.3 and 3.4 in the methods section.

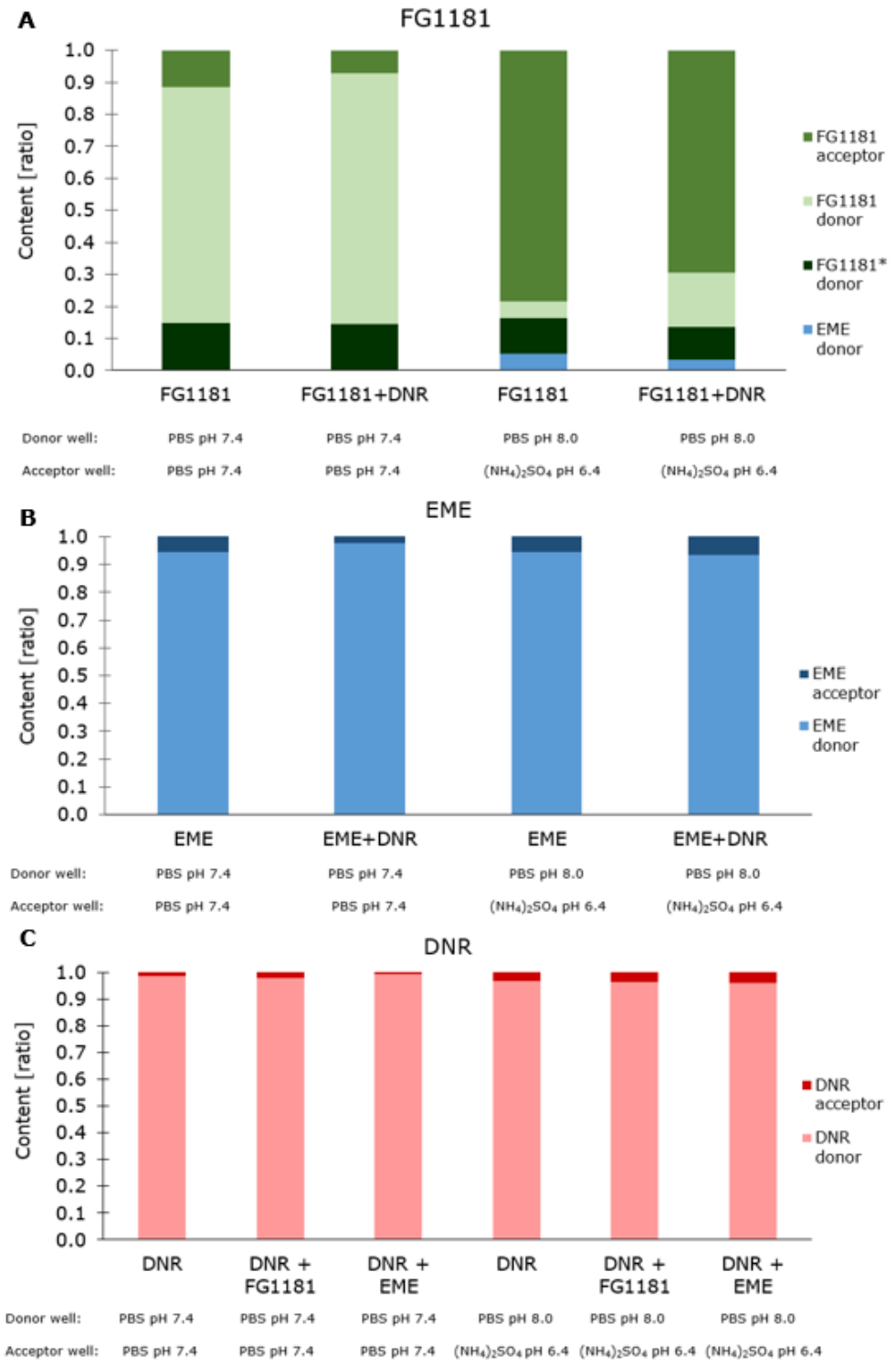

Figure 4.4 – Ability of compounds to cross phospholipid membranes. The bars represent the ratio of drugs present in the donor and acceptor wells of the PAMPA plate at different pH conditions in the acceptor and donor wells. The content of compounds was analyzed by RP-HPLC. **A**, **B**, and **C** represent the ratio of FG1181, Emetine (EME), and daunorubicin (DNR), respectively. The data presents the average of three experiments. For details on experimental conditions of the PAMPA and HPLC set-up, see chapters 3.4 and 3.3.3 in the methods section.

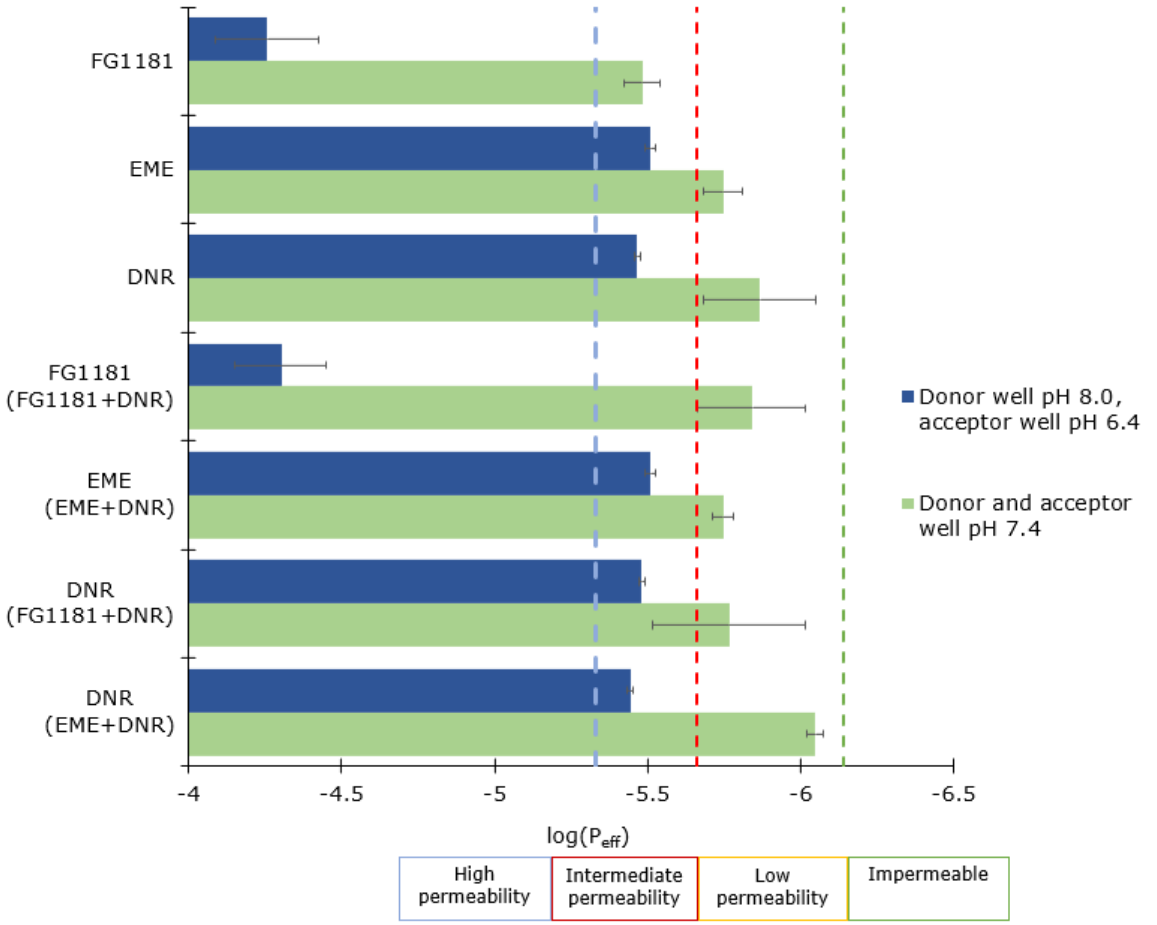

Figure 4.5 – Permeability of FG1181, emetine (EME) and daunorubicin (DNR) at different pH- conditions. The effective permeability P_{eff} was calculated from RP-HPLC-quantification data applied to Equation 3.3 and 3.4, as described in chapter 3.4 in the Method section. Log(P_{eff})< -6.14 is defined as impermeable, -6.14 < log(P_{eff})< -5.66 as low permeability, -5.66 < log(P_{eff})< -5.33 as intermediate permeability and log(P_{eff})over < -5.33 is considered as highly permeable (95).

Introduction of a substituent on the secondary amine of EME is reported to yield an inactive molecule. It was therefore imperative to demonstrate cytotoxic effect of FG1181 to prove the prodrug concept. A dose response cell assays for FG1181 and EME as free drug was performed to compare the potency and the timescale of the cytotoxicity. EC_{50} and T_{50} are the values of the half maximal effective concentration and time, respectively, where half of all the cells appear dead. Figure 4.6 shows the measured metabolic activity after 24-hours incubation and images acquired with a fluorescence microscope to manually count the percentage of living versus dead cells. The non-apoptotic nuclei appear as evenly stained and bean-shaped (green arrows in Figure 4.6 C), whereas apoptotic nuclei are more brightly stained, and are fragmented (red

arrows). At very high concentrations of EME or FG1181, the cells appeared to have disintegrated and very few cells were present in the wells (Figure 4.6 D). Note that EME is more potent and kills the cells faster than FG1181.

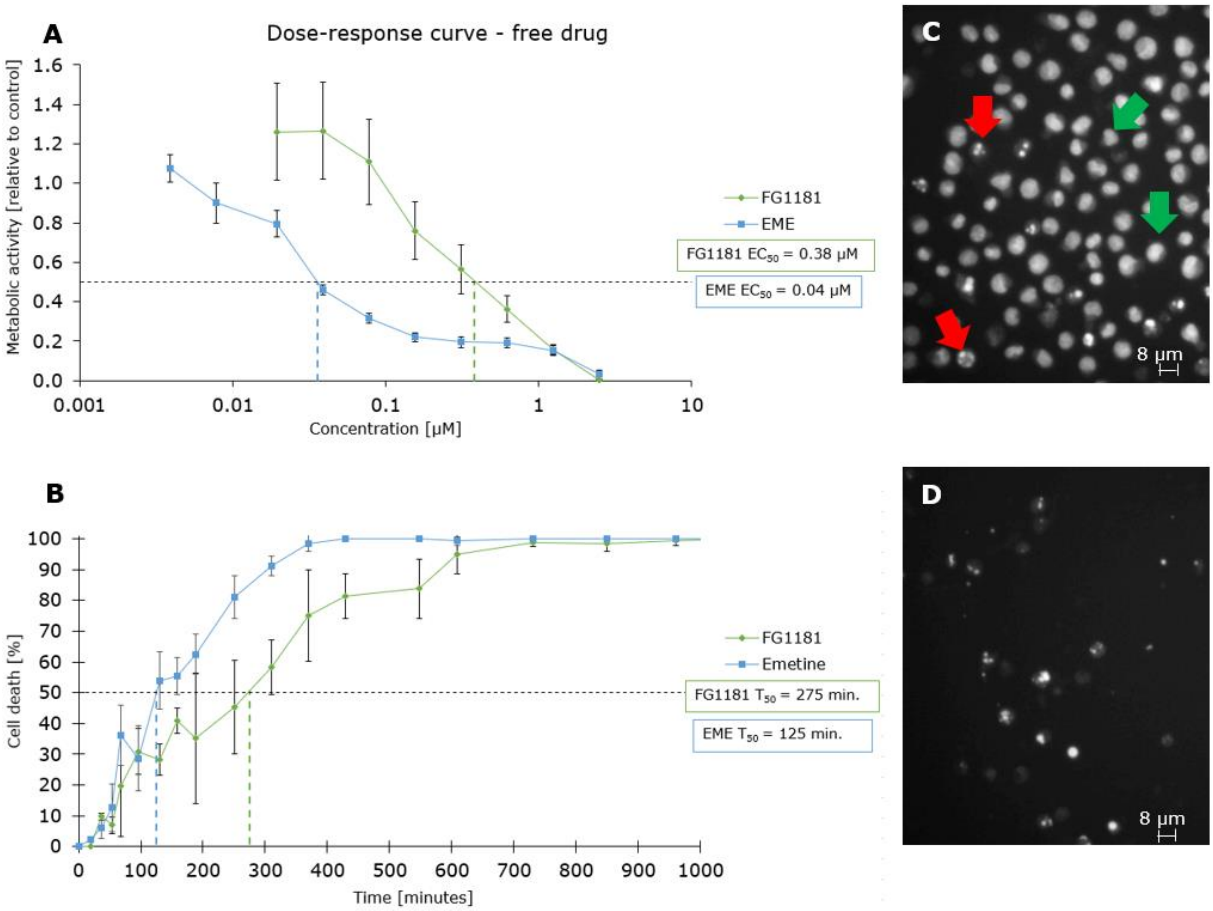

Figure 4.6 – Cytotoxicity of emetine and the analog FG1181 on MOLM13 AML cells. A, Dose-response curves comparing cell mortality after incubation for 24 hours and measuring of metabolic activity with the WST-1-reagent. The curves are averages of the three experiments performed in triplicates and standard deviation. **B,** Scheme showing a comparison of percentage apoptosis over time when treated with 2.5 µM FG1181 or 2.5 µM EME in a 24-hour kinetics assay described in chapter 3.5.3 in the Method section. Two images were acquired from each well, excluding images containing fewer than six cells. Each plot is an average of three experiments and standard deviation. The plots are adjusted for 30.49% cell death calculated from control. **C** and **D,** Images of untreated cells (**C**) and cells treated with FG1181 for 24 hours (**D**). Two examples of cells counted as apoptotic are marked with red arrows. Examples of cells counted as normal are marked with green arrows. Note that all the cells appear apoptotic in **D**.

FG1181, EME and DNR, alone and in combinations, were tested on the non-malignant cell lines NRK and H9c2 (Figure 4.7). This was done to evaluate each compound's cytotoxicity and estimate drug-related side-effects. The NRK cells appear to not be as affected as H9c2 by the treatment. A small beneficial effect for FG1181 compared to EME, alone and in combination with DNR, can be observed by the data.

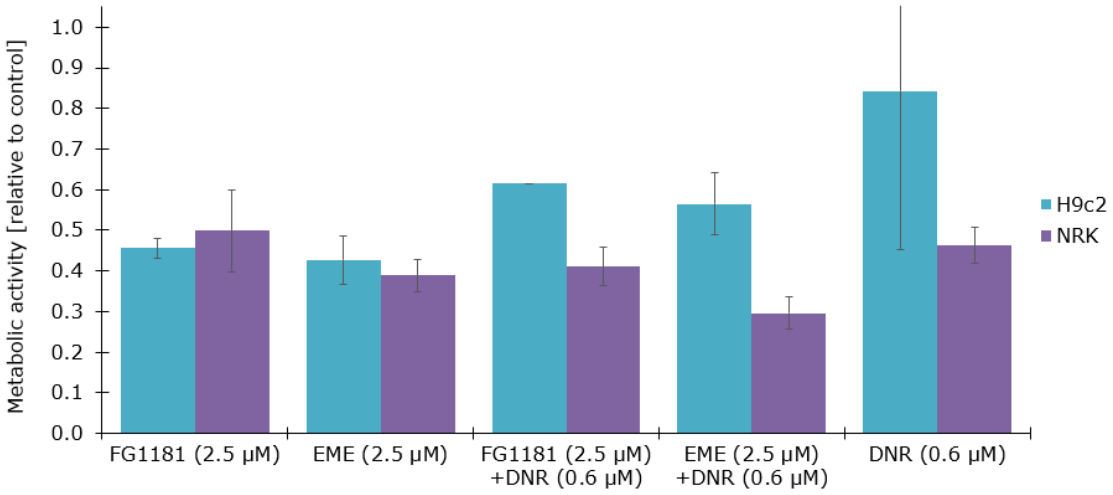

Figure 4.7 – Cytotoxicity of free drug on myocardium myoblast and kidney epithelial cells. 50 000 cells/mL were prepared in wells of a 96-well microplates 24 hours before free drug was added in concentrations given by the x-axis. The microplates were further incubated for 24 hours and metabolic activity evaluated using WST-1 reagent as described in chapter 3.5.2 of the Method section. The data is an average of three experiments.

4.2 Liposomal formulations

Liposomes containing DNR and EME has been shown to efficiently kill AML cell lines (23). We wanted to improve this by adding a prodrug of EME for delayed protein synthesis inhibition. Liposomes containing DNR, FG1181 or EME, or DNR in combination with EME or FG1181 were therefore produced. Four batches (A-D) were produced, here batch B and C were extruded with a gas extruder, and batch A and D with a syringe-driven mini extruder. Batch A was produced before FG1181 was available. The loading of the batch was performed with 1:10 compound-lipid weight ratio. Batch B had a larger average size because of some technical trouble with the gas extruder. For Batch B-D the loading of FG1181 and EME was performed with 1:5 compound-lipid weight ratio. Batch C was produced to compare liposomes loaded using shaking and heat and liposomes loaded overnight in the refrigerator. Batch D was produced with folate (DSPE-PEG(5000)folate). Further specifications of loading conditions are given in Figure 4.9.

4.2.1 Liposomal characteristics

The liposome sizes were measured in triplicates before and after loading to ensure that the liposomes were intact, and also had not agglomerated during drug loading or gel filtration (Figure 4.8). The PdI was < 0.078 for all measurements. The measured sizes and lipid content for the different batches are shown in Figure 4.9. The liposome sizes were measured in triplicates before and after loading to ensure that the liposomes were intact and had not agglomerated during compound loading or gel filtration. The lipid contents of the empty liposomes were calculated using Equation 3.1 after measurement with IR. For the liposomes containing DNR, a red band could be visibly detected as the loaded liposomes eluted from the SEC-column. The liposomes loaded with only EME or FG1181 were colorless, and to identify the liposomes, fractions were collected, and the lipid content measured.

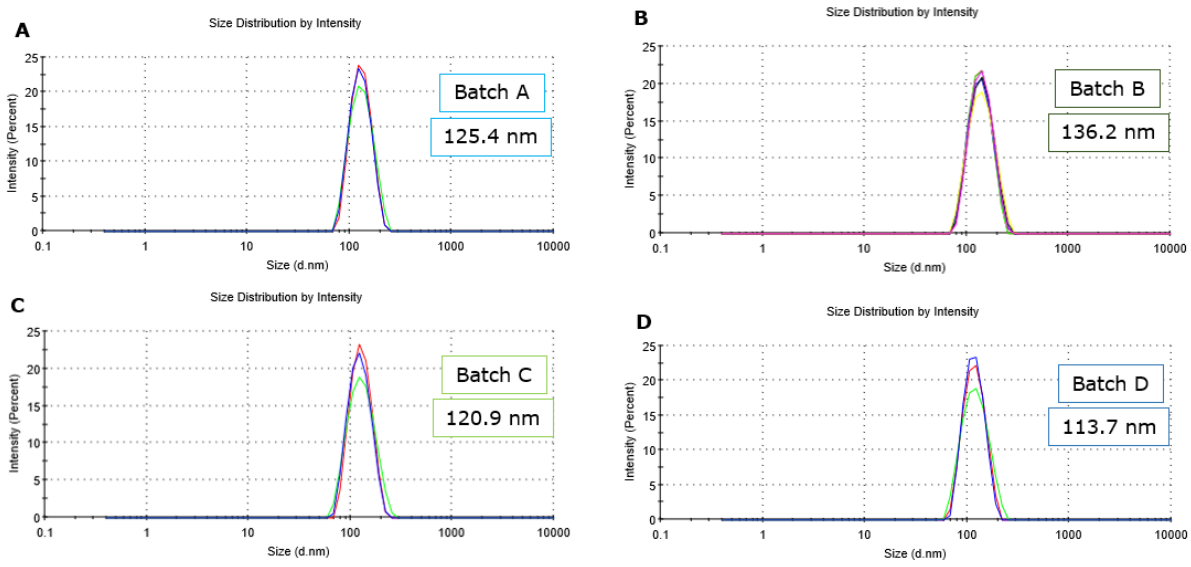

Figure 4.8 - Size distribution of empty liposomes after gel filtration. Size distribution measured with DLS. The schemes show three measurements.

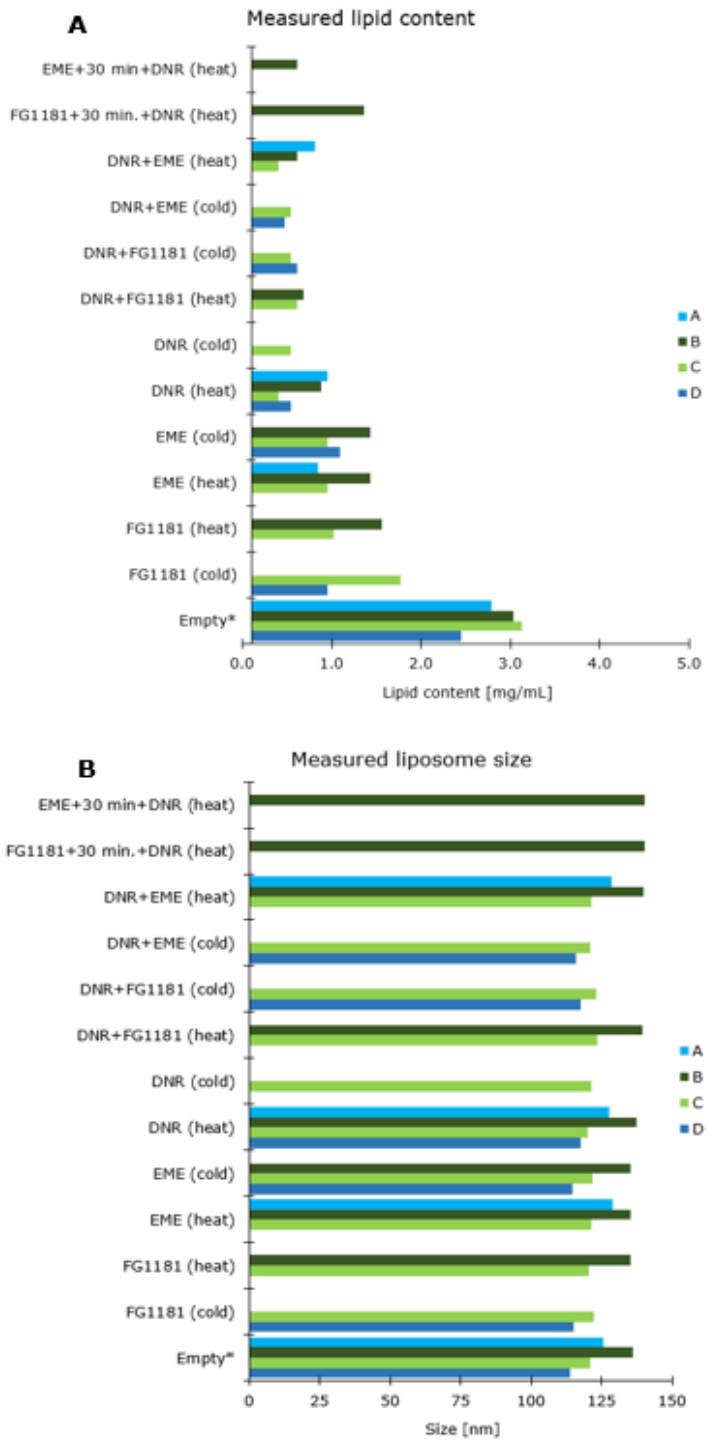

Figure 4.9 - Size and lipid content for the different liposome batches. Content of compounds and loading condition of the liposomes in the different batches are presented in the y-axes. The different batches are presented in different colors, as indicated. The blue indicates the batches produces with the mini-extruder and the green the batches produced with the gas-extruder. **A,** Lipid content measured with IR and calculated with Equation 3.1. **B,** Scheme of size measured with DLS for liposomes. The size is given as an average of three measurements of one sample after gel filtration. *The empty liposomes have a higher lipid content because they were only gel filtered once, compared to twice for the loaded liposomes.

4.2.2 Compound loading of liposomes

The gradients were changed after Batch B showed that the peaks for DNR and FG1181 were very close and could not be separated using the mobile phase composition and gradient conditions presented in Figure 3.1 A. Figure 4.10 shows spectrums before and after gradient adjustment. The measured compound loading based on the RP-HPLC standard curves is presented in Figure 4.11. EME and DNR were loaded better with incubation at 60℃, while FG1181 was better loaded overnight at 4℃. DNR appear to hinder the uptake of EME and FG1181 when incubated at 60℃, as illustrated in Figure 4.11 A.

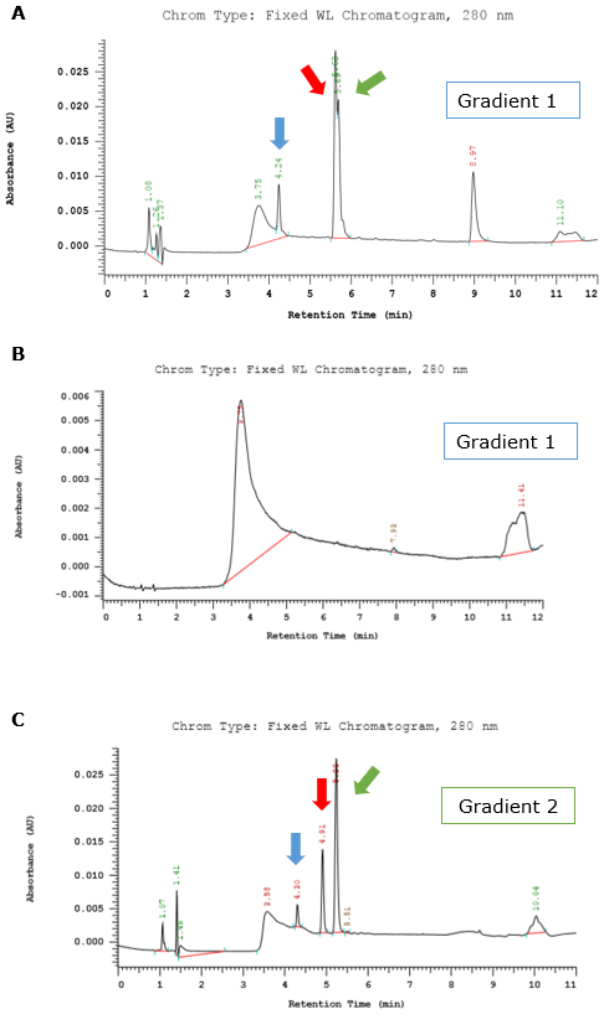

Figure 4.10 – Examples of RP-HPLC-spectra of compounds from liposomes. Emetine (EME) is marked in blue, FG1181 in green and daunorubicin (DNR) in red. **A,** Analysis of a liposomal formulation containing FG1181 and DNR from Batch B. The two peaks interject at t~5.60 minutes. Note the peak at t~4.20 minutes, indicating the presence of EME in the formulation. **B,** Example of a blank sample with gradient and background peaks at t ~3.75, t~7.93 and t~11.41 minutes. These peaks were not evaluated in the measurements. **C,** Spectrum of a liposomal formulation containing FG1181 and DNR in Batch C. Note that the DNR and FG1181 peaks have base-line separation due to the changed gradient (See Figure 3.1 in the Methods section) .

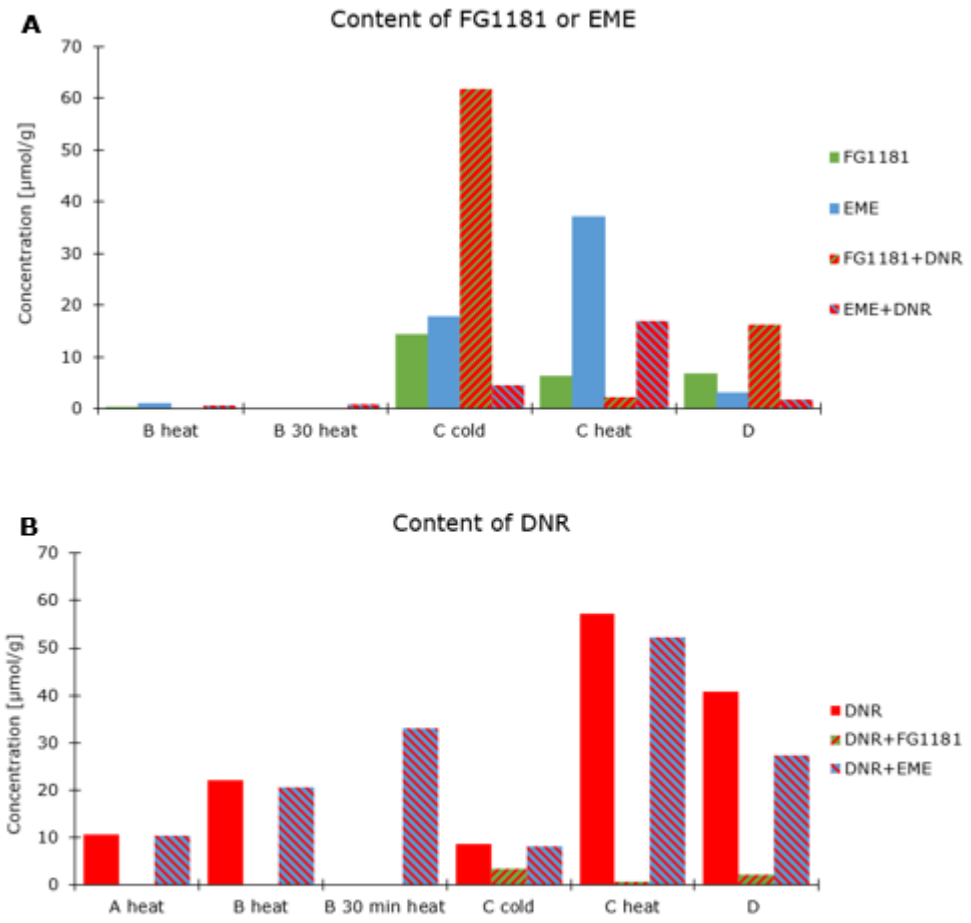

Figure 4.11 – Calculated compound loading for the liposomal formulations. The RP-HPLC standard curves were used to calculate compound loading. The x-axes specify batch and loading condition. **A,** Compound loading for FG1181 and EME liposomes. EME Batch A could not be quantified using RP-HPLC because of low compound content. **B,** Drug loading measured for the liposomes containing DNR. The loading of the combinations of FG1181 and DNR in Batch B is not given because of peak separation problems. The columns give the concentrations of DNR in the liposomal formulations.

After producing some of the liposomal batches, we developed a hypothesis of FG1181 being degraded by high temperature. To investigate, the content of FG1181 and EME in equally prepared samples stored at different temperatures were compared. The compound was tested alone and in combination with DNR. The samples were analyzed using RP-HPLC to find the content of EME. Figure 4.12 shows RP-HPLC-spectrums obtained and the results from the quantifications of the content of EME in the samples.

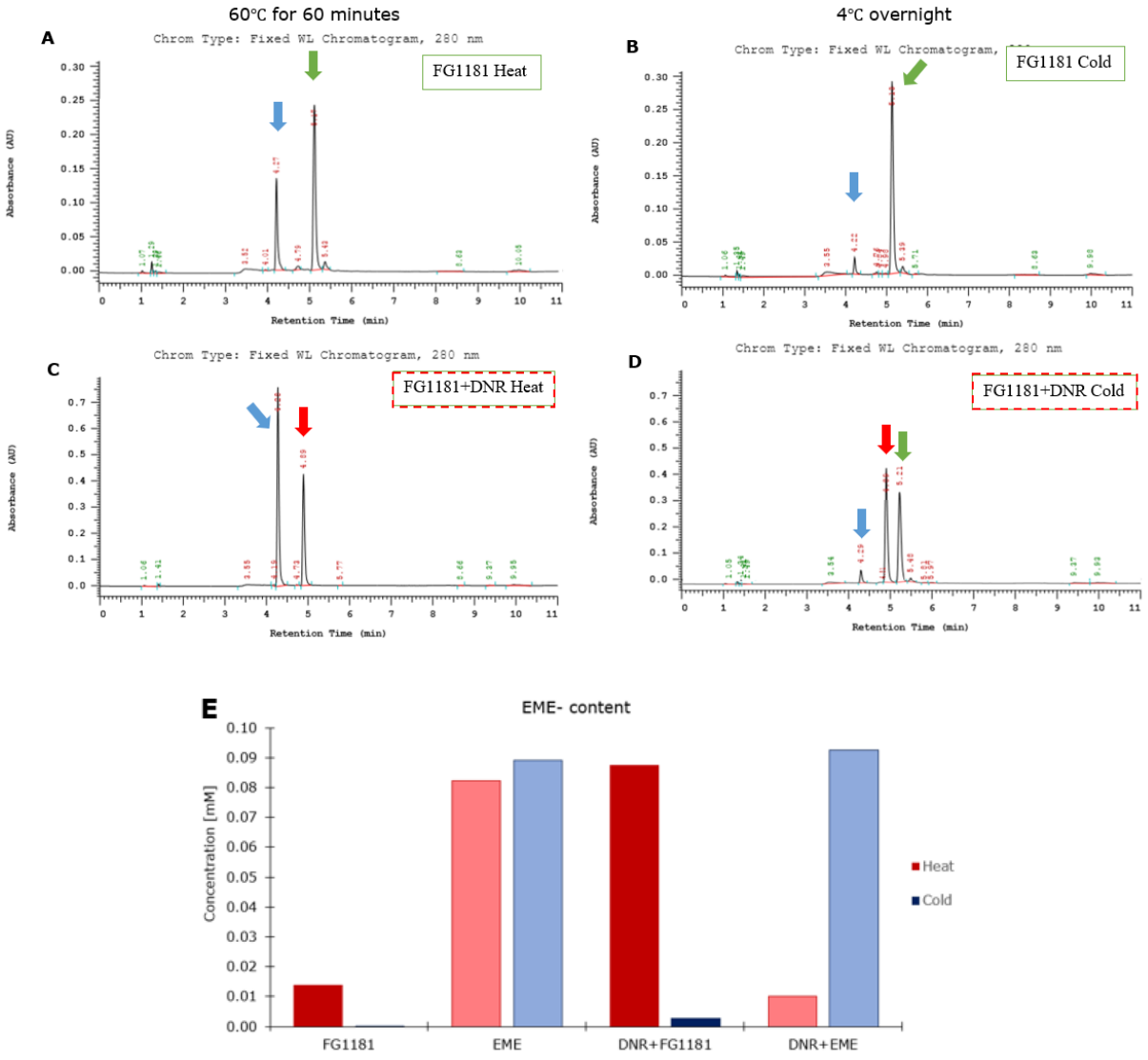

Figure 4.12 – Content of EME in equally prepared samples stored at different temperatures. Samples containing free compound were either shaken at 60°C for 60 minutes, illustrated in red, or stored dark at 4°C overnight, illustrated in blue in **E**. The bars give the concentration of EME in samples with composition specified in the x-axis. The light- colored bars indicate where EME should be found, while the dark-colored bars are FG1181 metabolized to EME. Note the difference between FG1181 alone and in combination with DNR. RP-HPLC was used to measure the contents in the samples. **A-D,** Spectrums of FG1181 alone treated with heat and cold, alone and in combination with DNR, respectively. EME is marked in blue, FG1181 in green and DNR in red. The content of each sample and storage condition is given in each figure.

All liposomal formulations were tested for cytotoxic potential towards MOLM13 cells. Dose response cell assays were performed to be able to compare EC_{50}-values. Empty liposomes from all batches were tested for cytotoxic effect on MOLM13 cells as shown in Figure 4.13. Figure 4.14 and 4.15 shows the cytotoxicity of free drug, as well as the different liposomal formulations and batches. Note the difference in EC_{50}-values in Figure 4.14, indicating a synergistic effect of FG1181 and DNR compared to that of DNR alone or in combination with EME. For the liposomal formulations, this is especially clear for batch B and C where the FG1181-combination has EC_{50}-values significantly lower than the EME-combination. The EC_{50}-value for DNR as free drug is here 0.074 µM, while the value for a combination of DNR and FG1181 or EME is 0.002 µM, which is 37 times decrease in dosage.

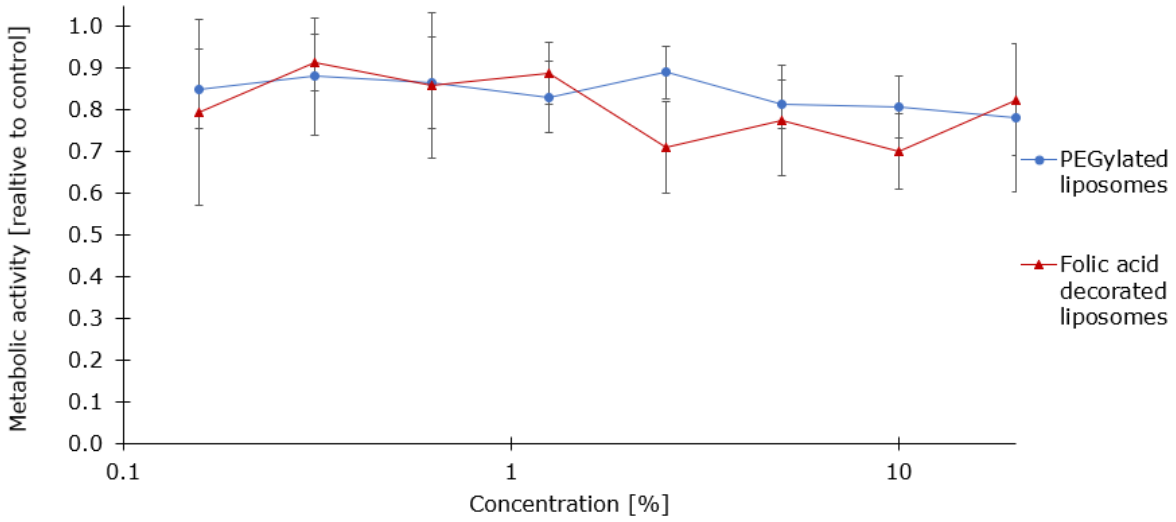

Figure 4.13 - Dose response cell assay with empty liposomes. Empty liposomes from every batch were tested on MOLM13 cells in three experiments. The scheme shows the average of Batches A-C and Batch D (folate). Twenty percent liposomal solution was added to the first well and diluted in a dose-response assay. The metabolic activity was measured after 24 hours of incubation utilizing WST-1 reagent. For details on cell assays, see chapters 3.5.2 in the methods section. The data on PEGylated liposomes represent average and standard deviation of three separate experiments performed on three separate batches, while the data on folate decorated liposomes are the average and standard deviation of three experiments on one batch.

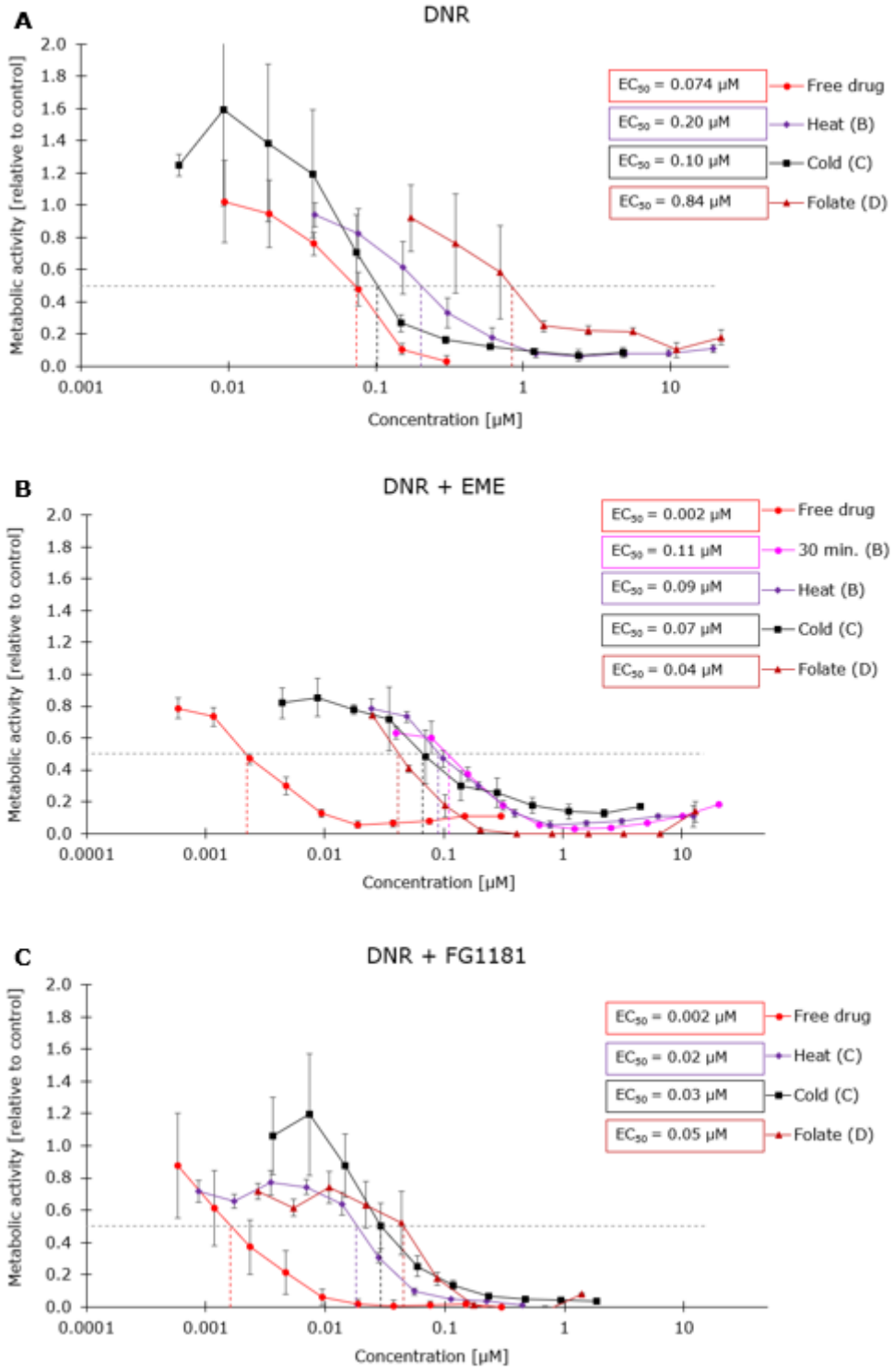

Figure 4.14 - Cytotoxicity of the different liposomal formulations and free compound combinations towards MOLM13 cells. All assays were performed in triplicates with standard deviation and incubated for 24 hours. The metabolic activity was measured with WST-1 reagent. Note that the plots are based on the concentration of DNR, not FG1181 or EME. See figure 4.11 A for concentration of FG1181 and EME in the different batches. **A,** Data from cell assays performed with DNR alone. **B,** Data from cell assays performed with a combination of DNR and EME. **C,** Data from cell assays performed with a combination of DNR and FG1181.

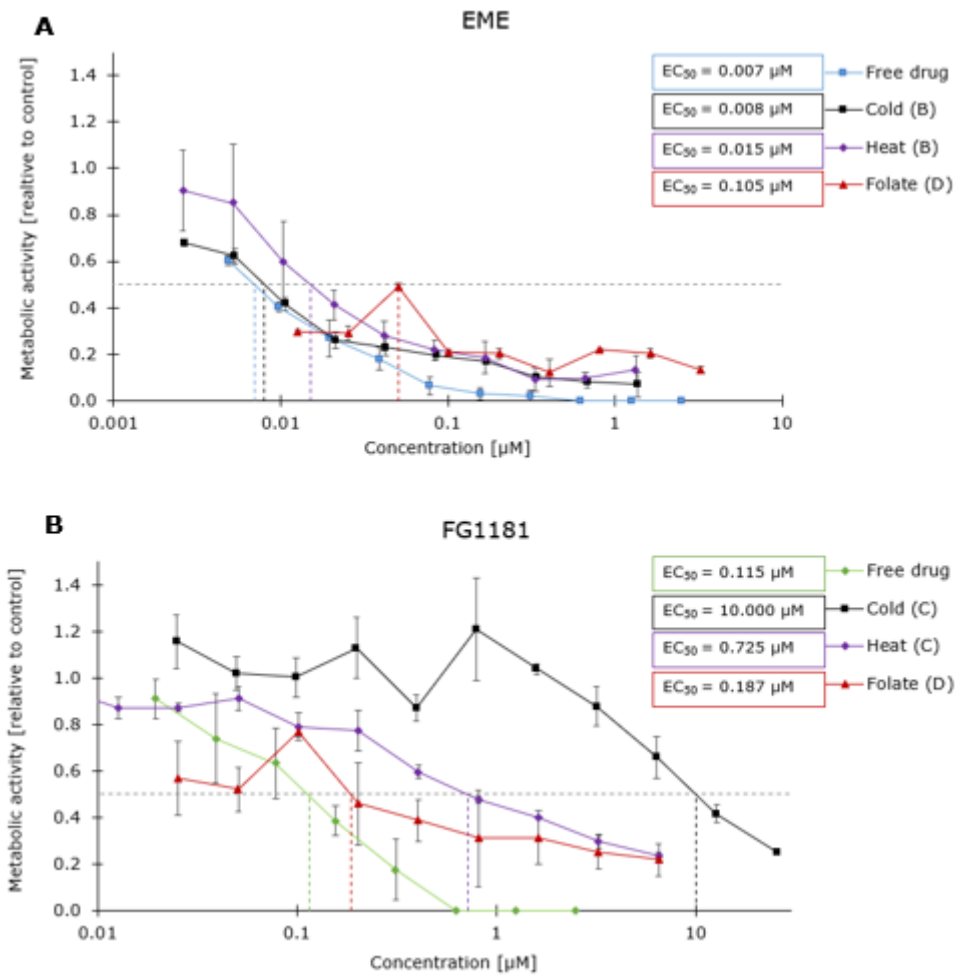

Figure 4.15 - Cytotoxicity of the different liposomal formulations and free compound towards MOLM13 cells. All assays were performed in triplicates with standard deviation and incubated for 24 hours. The metabolic activity was measured with WST-1 reagent. **A,** Data from cell assays performed with FG1181. **B,** Data from cell assays performed with EME.

4.2.3 Pulse test

A pulse test was performed with liposomes from Batch D (folate decorated liposomes). The test was performed because folate receptor targeting is most evident in short-term exposures and furthermore, we cannot assume that the liposomes are available for cellular uptake continuously for 24 hours (23). The results and experimental set ups are presented in Figure 4.16. The assays indicated that a short incubation was sufficient to produce a strong cytotoxic effect on the AML-cells. It also showed decreasing metabolic activity for the 60 minutes assay compared to the 30 minutes assay for the cells treated with liposomes loaded with FG1181 or DNR, and for the samples treated as shown in Figure 4.16 B. Note the different concentrations

given by the y-axes, as the assay were performed with equal volume of liposomal solution added to the cells, and not adjusted to produce equal concentrations of compounds.

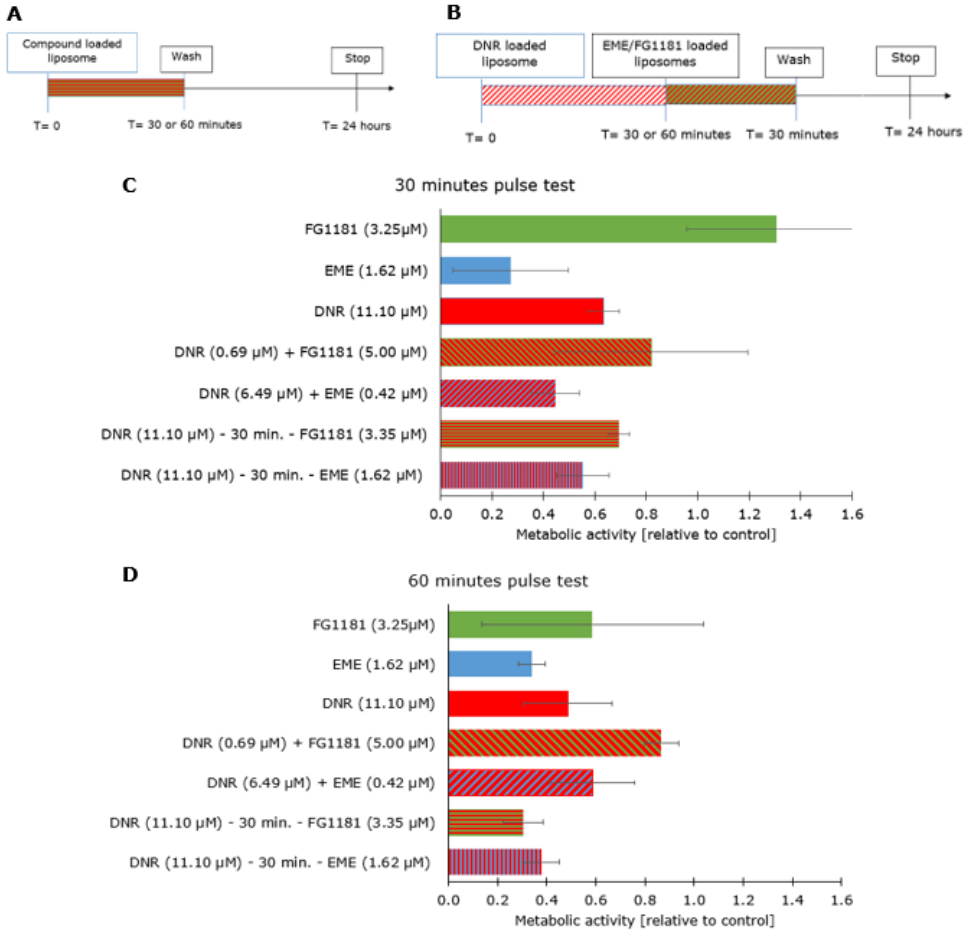

Figure 4.16 – Pulse cytotoxicity test of compound loaded folate decorated liposomes on MOLM13-cells. After treatment, the cells were incubated for a total of 24 hours and metabolic activity measured with WST-1 reagent. Note the difference in drug concentrations for the liposomes specified in the x-axes as the assays were performed with the same percentage of liposomal formulation, not compound concentration. **A** and **B,** Schematic presentation of the timelines of the assay. From the wash-step, the cells were spinned down and resuspended in fresh medium. **C** and **D,** Results from the 30 minutes and 60 minutes tests, respectively. The data are an average and standard deviation of three experiments.

5 Discussion

In this study, we evaluated the emetine (EME) analog FG1181 as a combination therapy with daunorubicin (DNR) against AML. The synergism with DNR and the novel analog FG1181 was compared to that of DNR and EME. Furthermore, successful loading of liposomes with FG1181 was achieved both alone and together with DNR. The efficacy of the compound loaded liposomes was demonstrated on the AML cell line MOLM13 and finally, we demonstrated that FG1181 and DNR were superior on MOLM13 AML cells compared to EME and DNR.

In silico predictions showed the protonation of the primary amine for FG1181 (Figure 4.1). However, after metabolization to EME, the compound can be further protonated on EME's secondary amine (green circle, figure 4.1 A). The peak apparent in the RP-HPLC spectra in Figure 4.3 at t~5:30-6:20 minutes can be hypothesized to degradation products of the two compounds. The RP-HPLC spectra in Figure 4.10 showed several gradient and background peaks which might have affected the readings, especially for EME at t~4.20 minutes, but not the noted peak. The large gradient peak at t~3.75 minutes in all spectra caused by the acetonitrile can be assumed to have influenced the readings to some degree, even though it was present at the standard curve, because it differs some in value and thereby impact the result. This would not be a problem if the concentration of EME was higher, as the peaks then would be larger and less affected. It must also be noted that using an autosampler would lead to more equal injections.

The different assays performed illustrates that there are differences between EME and FG1181 in terms of ionization, lipophilicity, membrane permeability, cytotoxicity and stability as illustrated in Figures 4.1, 4.5-4.7 and 4.13-4.16. PAMPA presented in Figures 4.3-4.5 was performed to estimate whether FG1181, EME and DNR cross the liposomal barrier passively. The different pH conditions affected all three compounds, but particularly FG1181. The acceptor wells with pH 6.4 contained between 70 and 80% of the FG1181 (Figure 4.4), and the calculated log(P_{eff})-values were -4.25 and -4.30, alone and in combination with DNR (Figure 4.5). These values show that the compound has high ability to cross membranes at the pH conditions where the majority of the compound is uncharged (Figure 4.1 and 4.5). Furthermore, the accumulation of FG1181 in the acceptor well suggest that the compound is trapped here presumably because the low pH protonates the primary amine (Figure 4.1). Both DNR and EME went from having low permeability to intermediate permeability when

comparing pH values of 7.4 to that of 8.0 in the donor and 6.4 in the acceptor wells (Figure 4.5). Although not as dramatic as for FG1181, there was a notable higher drug content in the acceptor wells corresponding to the increase in permeability.

For the PAMPA it must be noted that the membrane, unlike liposomes and cells, does not contain cholesterol. Cholesterol highly affects the stability and permeability of a membrane. This study shows, with the liposomal formulations that DNR and EME do cross the liposomal barrier given the same pH conditions as in the assay (PBS pH 8.0 and ammonium sulphate pH 6.4). This highlights the fact that a pre-made PAMPA can only be used as an indicator for membrane permeability. Furthermore, the PAMPA was performed at room temperature, which did not exceed the membrane's transition temperature. Still, we noted that with the same pH gradient as in the liposomes, there was an increase in permeability from -5.86 to -5.67 ($\log(P_{eff})$-values) for DNR alone (Figure 4.5) and an increase in the content in the acceptor well of 38% (Figure 4.4).

The dose response and kinetics curves shown in Figure 4.6 compare the cytotoxic potential of FG1181 and EME as free compounds. They show that EME has lower EC_{50} and T_{50}, compared to FG1181. Both compounds reach complete cell death at the same concentration (2.5 µM) after 24 hours (Figure 4.6 A). The difference in EC_{50}-values could be explained by FG1181 being less potent than EME. It can also be caused by the desired prodrug effect, meaning that it was degraded to the active compound EME after a certain time period. This was supported by the kinetics assay showing that the T_{50}-value of FG1181 appeared approximately 150 minutes after that of EME. In the assay, FG1181 used approximately 18 hours to reach complete cell death compared to 12 hours for EME. This might be caused by FG1181 being more lipophilic than EME, leading to the possibility of it binding to lipophilic binding site in plasma protein or lipoprotein and being less available for uptake in cells. Incorporating FG1181 in liposomes will protect the compound from these bindings, thereby leading to a higher uptake of the compound into the cells. For the free compound in Figure 4.15, a higher EC_{50}-value is observed compared to the liposomal formulations, but this might be caused by degradation to a more active EME. However, to fully establish that FG1181 is inactive and converted to active EME either in medium or intracellularly, liquid chromatography-mass spectroscopy (LC-MS) analyses of the compounds from cell lysates could be made. It must be noted that the control well in the time kinetics assay has an unusual high level of cell death. However, as the assay was performed using microscopy, the exact cell count of each well is not relevant.

FG1181 showed lower toxicity towards non-malignant cell lines compared with EME, both alone and in combination with DNR (Figure 4.7). This can be interpreted as an FG1181 being less cytotoxic for these cell lines and thereby will lead to less drug-related side-effects, for instance cardiomyopathy. DNR shows less toxicity for the H9c2 cell line alone at the given dose. However, the color of DNR interferes with the assay and high DNR concentrations might give positive results for metabolic activity, but for comparing DNR alone or in combination with a protein synthesis inhibitor, the color effect of DNR is expected to be equal. A decrease in side-effects would improve the treatment of AML, especially for frailer patients that do not tolerate the current treatment methods.

Different conditions for liposomal production and drug loading were tested to find which method gave the optimal result with respect to size distribution and compound loading. The size distribution between the batches varied little, being between 113.7 nm and 140.4 nm (Figure 4.8 and Figure 4.9), which correlates well with clinical recommendations (53). Batch B, produced with the gas extrusion, gave the largest liposomes with the highest measured lipid content after the second gel filtering probably due to a faulty filter. The liposomal formulations with a combination of EME/FG1181 and DNR were shown to be larger than single compound loaded liposomes in average (Figure 4.9).

RP-HPLC of the liposomal batches showed that more EME was loaded into the liposomes using incubation at 60°C, compared to diffusion overnight in the dark at 4°C (Figure 4.11). This correlates well with the data from the PAMPA plate (Figures 4.4 and 4.5), which showed that FG1181 diffused over the membrane passively to a greater extent than EME. Both EME and DNR showed a higher degree of loading at temperatures exceeding the phase transition temperature of the lipid membrane (Figure 4.11). However, loading of both FG1181 and DNR proved difficult because of difference in optimal loading conditions. Studies showed that FG1181 seemed to be degraded to EME at high temperatures (≥ 60°C). The PAMPA was performed at room temperature and the loading at ≥ 60°C, which might have affected FG1181 as further temperature studies (Figure 4.12) showed that the compound is highly affected by increased temperature (≥ 60°C). When comparing the FG1181 samples illustrated in Figure 4.12, it became apparent that more EME was present in the sample incubated at 60°C for one hour compared to the samples incubated at 4°C overnight. For the heat-treated sample containing a combination of FG1181 and DNR, no FG1181 was detected compared to 0.2 µM for the sample stored in the dark at 4°C, suggesting that the presence of DNR facilitated

degradation of FG1181. It was also shown that more FG1181 was metabolized in the presence of DNR compared to alone (Figure 4.12).

A compound´s lack of tolerance to temperature change can greatly affect its clinical use. As FG1181 has here been shown to be less stable at increased temperatures (≥ 60℃), but with unknown response to room temperature, the handling of a potential drug formulation before administrations needs to be done with extra care. Some cytostatics are prepared and heated before infusion to avoid discomfort for the patient, but in this case FG1181 would have to be prepared, stored and infused cold, perhaps as a freeze dried powder. The cytostatic Bortezomib is an example of an infusion in clinical use that needs to be administered no more than eight hours after reconstitution because it is unstable at room temperature (109). However, it must be emphasized that the purpose of this study was to develop a suggestion for improved treatment of AML, not to produce a standard operating procedure to produce a specific drug. The study was not performed at a pharmaceutical production facility, and some expected batch variations were observed.

In Figure 4.11, "DNR+FG1181" was loaded overnight in the dark at 4℃ for Batch C (cold) and Batch D (folate decorated liposomes). These show a lower drug concentration than the batches loaded by incubation at 60℃. It must be noted that "EME+DNR" and DNR were loaded by heat incubation at 60℃ in Batch D, and therefore have a higher DNR concentration compared to "FG1181+DNR" which was loaded in the dark at 4℃. In the future, one might try to load the liposomes with DNR at 60℃ first, then cool the liposomal formulation down, before adding FG1181 in the dark overnight at 4℃. This might improve the loading. On the other hand, DNR seem to obstruct the uptake of EME and FG1181 when loaded at 60℃, which might indicate that this sequncial loading might not improve the uptake of compound (Figure 4.16).

An attempt of first loading liposomes with FG1181/EME for 30 minutes and then add DNR produced liposomes which were cytotoxic, but quantification by RP-HPLC was not successful for the FG1181 batch due to the lack of baseline separation of peaks (Figure in Appendix II). The liposomes first loaded with EME and then DNR did not show any improved loading for EME. The hypothesis was that by incorporating FG1181 into the liposomes first, the compound would be protected from degradation by DNR and ensure a higher uptake. The RP-HPLC spectrum (Appendix II) showed little EME in this sample compared to that found in Figure 4.13 A where DNR and FG1181 were loaded together. This indicates that the liposomes protect

the FG1181 from being degraded by DNR and correlates well with the data from the PAMPA plate (Figure 4.4), which showed no EME in the FG1181 acceptor wells with pH 6.4, which can be compared to the interior of the liposomes.

The liposomes loaded with DNR at 60°C showed less variation in drug compared to liposomes loaded with EME and FG1181 alone. This can be partly explained by the liposomes loaded with DNR being colored red, thereby making them easier to detect during gel filtration. This became apparent for the folate decorated liposomes which had lower loading of FG1181 and EME compared to the PEGylated liposomes (Figure 4.11). The folate might have interfered with the compound loading, or the fractionation of liposomes loaded with the clear compounds might have been unsuccessful. The same column was used for all gel filtrations and was thoroughly rinsed between every filtration, but it would be optimal to have separate columns for each formulation to ensure that no compound was transferred. In many cases, targeted nanocarriers are added to the targeting ligand after production. It is therefore possible to first load the liposomes with drugs, and then add the targeting moieties, either small molecules or antibodies (110). This will prevent that surface molecules reduce loading efficiency. For the liposomal formulation created overnight at 4°C, Batch D (folate decorated liposome), the EC_{50}-value of FG1181 was lower than that of EME, contrary to what was seen with non-folate liposomes (Figure 4.15). One explanation for this can be that FG1181 was degraded to EME during preparation of the liposomes, and that EME is the main constituent of these liposomes.

When comparing the results from DNR alone and in combination with a protein synthesis inhibitor, the combination appears favorable (Figure 4.14), which correlates well with earlier data (23, 47, 57). For free drug, EC_{50}-values were 0.07 µM for DNR alone and 0.002 µM for DNR in combination with EME or FG1181 of different concentrations. Overall, FG1181 shows promising results for synergistic use with DNR. The EC_{50}-values for the folate covered liposomes was almost twenty-fold higher for DNR alone compared to the combination of both FG1181 and EME (Figure 4.14). Both the batch incubated at 60°C and the batch incubated at 4°C favors FG1181 (Figure 4.14 B and C).

The pulse test was performed because in the circulating blood or in the bone marrow, the AML blasts might not be exposed to the liposomes continuously for 24 hours as is the case with our cell experiments. In order to mimic a shorter exposure time, we exposed the MOLM13 cells to the liposomes for a short pulse of 30 or 60 minutes, followed by wash and further incubation in a drug free medium for another 23 hours (Figure 4.16). Increased

cytotoxicity was observed for the 60-minutes assay compared to the 30-minutes assay, but the assays both had substantial standard deviation. However, earlier research has shown that a short exposure period of liposomes is enough to ensure effect (111). As shown in Figure 4.14, the same concentration of DNR in the folate decorated liposomes gave a metabolic activity of 0.18 relative to control, while it in the pulse test in Figure 4.16 gives values of 0.63 and 0.48 for the 30- and 60-minutes assay, respectively. Liposomes containing both FG1181 and DNR did not show an increase in cell death compared to liposomes with DNR in Figure 4.16, but the low concentration of DNR in the combination liposomes must be noted. For future investigations, the test should be performed with the same compound concentration instead of identical liposomal concentrations.

We also wanted to investigate whether FG1181 and EME had equal effects on cellular signaling, and studied cleavage of Caspase 3, an indication of apoptosis with Western blot. However, the results, presented in Appendix I, were inconclusive.

6 Concluding remarks and further investigations

The aims of this master thesis were to investigate the biological activity of FG1181 and compare it to that of emetine (EME), incorporate it in liposomes and investigate synergism with daunorubicin (DNR). The combination of DNR and FG1181 appears to be beneficial for the patient, both as free drug and incorporated into liposomes. FG1181 was showed to have a time delayed cytotoxicity compared to EME, but its temperature instability can pose a problem in the production and handling of the liposomal formulation. Small molecules, here liposomes, show promising results in the field of cancer therapy and could be expected to decrease drug-related side-effects.

For further investigations, other analogs of EME could be developed to see if more heat-stable molecules could be produced. A more heat stable analog with prodrug effect would be easier to handle in the production and for administration of the liposomal formulation. It would also be easier to obtain sufficient and reliable loading of the liposomes with both DNR and an EME analog if the temperature could exceed the phase transition temperature of the liposomal membranes. Further temperature studies of the FG1181 could have been performed, for instance by loading the compound into liposomes at room temperature and at other temperatures to investigate if this led to a higher degree of compound loading.

For future investigations, we would have liked to perform the pulse test with the same concentration of compound and in a dose-response assay with decreasing concentrations. It would be interesting to test liposomal formulations on the non-malignant cell lines and do a kinetics assay with liposomal FG1181 to compare with the results found for free drug. The kinetics assay could also have been repeated with the compounds' EC_{50}-concentrations. We would have liked to investigate and compare more ways to load FG1181 into liposomes, for instance by first loading FG1181 into the liposomes in the dark at 4℃ overnight and then load DNR at 60℃ for one hour, or vice versa with cooling the formulation to 4℃ before adding FG1181. LS-MS could be used to establish whether FG1181 is in fact an inactive compound being converted into a more active EME.

Finally, the documentation provide in this thesis for a prodrug of EME for delayed activity is sufficient to pursue the concept in animal models of AML. If efficacy can be demonstrated in for instance a mouse AML xenograft model, it could very well be that the pharmaceutical industry sees potential in this treatment strategy.

References

1. Leukemia. Encyclopedia of Genetics, Genomics, Proteomics and Informatics. Dordrecht: Springer Netherlands; 2008. p. 1097-9.
2. Jagannathan-Bogdan M, Zon LI. Hematopoiesis. Development (Cambridge, England). 2013;140(12):2463.
3. Döhner H, Weisdorf DJ, Bloomfield CD. Acute myeloid leukemia. New England Journal of Medicine. 2015;373(12):1136-52.
4. Cumpston, Craig AM. Acute Leukemia. 2014. p. 307-20.
5. Jamieson CHM, Weissman IL, Passegué E. Chronic versus acute myelogenous leukemia:A question of self-renewal: A question of self-renewal. Cancer Cell. 2004;6(6):531-3.
6. Zhou J, Chng W-J. Identification and targeting leukemia stem cells: The path to the cure for acute myeloid leukemia. Beijing, China :2014. p. 473-84.
7. Lara W, George QD. Progress towards generation of human haematopoietic stem cells. Nature Cell Biology. 2016;18(11).
8. Hiddemann W. Handbook of Acute Leukemia. Cham: Springer International Publishing : Imprint: Adis; 2016.
9. Helsedirektoratet. Nasjonalt handlingsprogram med retningslinjer for diagnostikk, behandling og oppfølging av maligne blodsykdommer [Internet]. Oslo: Helsedirektoratet; 2018 [updated Sep 2018; cited 2018 Oct 1st]. Available from: https://helsedirektoratet.no/Lists/Publikasjoner/Attachments/1470/IS-2746_Nasjonalt%20handlingsprogram%20for%20maligne%20blodsykdommer.pdf.
10. Sauvage F, Barratt G, Herfindal L, Vergnaud-Gauduchon J. The Use of Nanocarriers in Acute Myeloid Leukaemia Therapy: Challenges and Current Status. Curr Pharm Biotechnol. 2016;17(1):30-41.
11. Helsedirektoratet. Pakkeløp for akutt leukemi [Internet]. Helsedirektoratet; 2018 [updated Jun 9th 2018]; cited 2018 Sep 9th]. Available from: https://helsedirektoratet.no/Retningslinjer/Akutt%20leukemi%20%E2%80%93%20pakkeforl%C3%B8p.pdf.
12. American Cancer Society®. Cancer Facts & figures 2018 Atlanta: American Cancer Society®; 2018 [cited 2018 Sep 9th]. Available from: https://www.cancer.org/content/dam/cancer-org/research/cancer-facts-and-statistics/annual-cancer-facts-and-figures/2018/cancer-facts-and-figures-2018.pdf.

13. Cancer Research UK. Acute myeloid leukaemia (AML) incidence by age 2018 [updated 24 January 2018; cited 2019 May 9th]. Available from: https://www.cancerresearchuk.org/health-professional/cancer-statistics/statistics-by-cancer-type/leukaemia-aml/incidence#heading-One.

14. Singh A, Myklebust NN, Furevik SMV, Haugse R, Herfindal L. Immunoliposomes in acute myeloid leukaemia therapy. An overview of possible targets and obstacles. 2019.

15. Howlader N, Noone A, Krapcho M, Miller D, Bishop K, Altekruse S, et al. SEER cancer statistics review, 1975–2013. Bethesda, MD: National Cancer Institute. 2016;19.

16. Statistisk sentralbyrå (Statistics Norway). Deaths 2019 [updated March 7th, 2019; cited 2019 May 14th]. Available from: https://www.ssb.no/en/befolkning/statistikker/dode/aar.

17. European Medicines Agency. Vyxeos 2018 [updated Oct 26th 2018; cited 2019 May 15th]. Available from: https://www.ema.europa.eu/en/medicines/human/EPAR/vyxeos.

18. Juliusson G, Lazarevic V, Hörstedt A-S, Hagberg O, Höglund M. Acute myeloid leukemia in the real world: why population-based registries are needed. Blood. 2012;119(17):3890-9.

19. Rowe JM, Tallman MS. How I treat acute myeloid leukemia. Blood. 2010;116(17):3147-56.

20. Kadia TM, Ravandi F, Apos, Brien S, Cortes J, Kantarjian HM. Progress in Acute Myeloid Leukemia. Clinical Lymphoma Myeloma and Leukemia2015. p. 139-51.

21. Lima AS, de Mello MR, Fernandes E, Bezerra MF, Oliveira MM, Duarte BK, et al. Clinical outcomes of patients with acute myeloid leukemia: evaluation of genetic and molecular findings in a real-life setting. Blood. 2015;126(15):1863-5.

22. De Kouchkovsky I, Abdul-Hay M. Acute myeloid leukemia: a comprehensive review and 2016 update. Blood Cancer Journal. 2016;6:e441.

23. Myhren L, Nilssen IM, Nicolas V, Døskeland SO, Barratt G, Herfindal L. Efficacy of multi-functional liposomes containing daunorubicin and emetine for treatment of acute myeloid leukaemia. Eur J Pharm Biopharm. 2014;88(1):186-93.

24. Grimwade D, Hills RK. Independent prognostic factors for AML outcome. Hematology American Society of Hematology Education Program. 2009;2009(1):385.

25. Arber DA, Orazi A, Hasserjian R, Thiele J, Borowitz MJ, Le Beau MM, et al. The 2016 revision to the World Health Organization classification of myeloid neoplasms and acute leukemia. Blood. 2016;127(20):2391.

26. Walter RB, Othus M, Burnett AK, Löwenberg B, Kantarjian HM, Ossenkoppele GJ, et al. Significance of FAB subclassification of "acute myeloid leukemia, NOS" in the 2008 WHO classification: analysis of 5848 newly diagnosed patients. Blood. 2013;121(13):2424.

27. Mrozek K, Marcucci G, Nicolet D, Maharry KS, Becker H, Whitman SP, et al. Prognostic significance of the European LeukemiaNet standardized system for reporting cytogenetic and molecular alterations in adults with acute myeloid leukemia. J Clin Oncol. 2012;30(36):4515-23.

28. Wang A, Langer R, Farokhzad O. Nanoparticle Delivery of Cancer Drugs. Annual Review of Medicine. 2012;63:185.

29. Ferrara F, Schiffer CA. Acute myeloid leukaemia in adults. Lancet (London, England). 2013;381(9865):484.

30. Döhner H, Estey E, Grimwade D, Amadori S, Appelbaum F, Büchner T, et al. Diagnosis and management of AML in adults: 2017 ELN recommendations from an international expert panel. Blood. 2017;129(4):424-47.

31. Burnett A, Wetzler M, Löwenberg B. Therapeutic advances in acute myeloid leukemia. Journal of clinical oncology : official journal of the American Society of Clinical Oncology. 2011;29(5):487.

32. Brinch L. Allogen stamcelletransplantasjon med ikke-myeloablativ kondisjonering Oncolex.no: Oncolex; [cited 2019 May 30th]. Available from: http://oncolex.no/PROSEDYRER-ONCOLEX/BEHANDLING/Medikamentell-behandling/Leukemi-mini-tx?procedureSearchText=stamcelle.

33. Bulbake U, Doppalapudi S, Kommineni N, Khan W. Liposomal Formulations in Clinical Use: An Updated Review. Pharmaceutics. 2017;9(2):12.

34. Crain LM. Daunorubicin & Cytarabine Liposome (Vyxeos™). Oncology Times. 2018;40(10):30-.

35. U.S. National Library of Medicine. ClinicalTrials.org CPX-351 2019 [cited 2019 May 14th]. Available from: https://clinicaltrials.gov/ct2/results?cond=&term=CPX-351&cntry=&state=&city=&dist=.

36. Potocnik J. Commission recommendation of 18 October 2011 on the definition of nanomaterial. Off J Eur Union L. 2011;275:38-40.

37. Schutz CA, Juillerat-Jeanneret L, Mueller H, Lynch I, Riediker M, NanoImpactNet C. Therapeutic nanoparticles in clinics and under clinical evaluation. Nanomedicine (Lond). 2013;8(3):449-67.

38. Anselmo AC, Mitragotri S. Nanoparticles in the clinic. Bioeng Transl Med. 2016;1(1):10-29.

39. European Medicines Agency. SonoVue 2007 [updated May 25th 2018; cited 2019 May 15th]. Available from: https://www.ema.europa.eu/en/medicines/human/EPAR/sonovue.

40. European Medicines Agency. Abraxane 2009 [updated May 11th 2015; cited 2019 May 15th]. Available from: https://www.ema.europa.eu/en/medicines/human/EPAR/abraxane.

41. Wicki A, Witzigmann D, Balasubramanian V, Huwyler J. Nanomedicine in cancer therapy: Challenges, opportunities, and clinical applications. Journal of Controlled Release. 2015;200:138-57.

42. Dan P, Jeffrey MK, Seungpyo H, Omid CF, Rimona M, Robert L. Nanocarriers as an emerging platform for cancer therapy. Nature Nanotechnology. 2007;2(12):751.

43. Williams HD, Trevaskis NL, Charman SA, Shanker RM, Charman WN, Pouton CW, et al. Strategies to Address Low Drug Solubility in Discovery and Development. Pharmacological Reviews. 2013;65(1):315-499.

44. Deutsch YE, Presutto JT, Brahim A, Raychaudhuri J, Ruiz MA, Sandoval-Sus J, et al. Safety and Feasibility of Outpatient Liposomal Daunorubicin and Cytarabine (Vyxeos) Induction and Management in Patients with Secondary AML. Blood. 2018;132(Suppl 1):3559-.

45. Bae KHKAIoS, Technology DRoK, Chung HJKAIoS, Technology DRoK, Park TGKAIoS, Technology DRoK. Nanomaterials for Cancer Therapy and Imaging. Nanomaterials for Cancer Therapy and Imaging. 2011(4):295-302.

46. Benasutti H, Wang G, Vu VP, Scheinman R, Groman E, Saba L, et al. Variability of Complement Response toward Preclinical and Clinical Nanocarriers in the General Population. Washington, D.C. :2017. p. 2747-55.

47. Suk JS, Xu Q, Kim N, Hanes J, Ensign LM. PEGylation as a strategy for improving nanoparticle-based drug and gene delivery. Advanced Drug Delivery Reviews. 2016;99(Pt A):28-51.

48. Gabizon A, Shmeeda H, Barenholz Y. Pharmacokinetics of Pegylated Liposomal Doxorubicin. Clinical Pharmacokinetics. 2003;42(5):419-36.

49. Lyass O, Uziely B, Ben-Yosef R, Tzemach D, Heshing NI, Lotem M, et al. Correlation of toxicity with pharmacokinetics of pegylated liposomal doxorubicin (Doxil) in metastatic breast carcinoma. Cancer: Interdisciplinary International Journal of the American Cancer Society. 2000;89(5):1037-47.

50. Patel HM. Liposomes: A practical approach: Edited by R.R.C. New; Oxford University Press; Oxford, 1990; 301 pages. 1990.
51. Bozzuto G, Molinari A. Liposomes as nanomedical devices. International Journal of Nanomedicine. 2015;2015:975-99.
52. Herfindal L, Nilssen IM, Milankovic S. Nanokolloidar som verktøy for å betra distribusjon av legemiddel. Naturen. 2012;136(03):103-9.
53. Litzinger DC, Buiting A, Vanrooijen N, Huang L. Effect of liposome size on the circulation time and intraorgan distribution of amphipathic poly(ethylene glycol)-containing liposomes. Biochim Biophys Acta-Biomembr. 1994;1190(1):99-107.
54. Pelengaris S, Pelengaris SM, Khan MM. The molecular biology of cancer. S.l.]: S.l. : WILEY; 2009.
55. Tang W-L, Tang W-H, Li S-D. Cancer theranostic applications of lipid-based nanoparticles. Drug Discovery Today. 2018;23(5):1159-66.
56. Danhier F. To exploit the tumor microenvironment: Since the EPR effect fails in the clinic, what is the future of nanomedicine? Journal of Controlled Release. 2016;244(Pt A):108-21.
57. Gausdal G, Gjertsen BT, McCormack E, Van Damme P, Hovland R, Krakstad C, et al. Abolition of stress-induced protein synthesis sensitizes leukemia cells to anthracycline-induced death. Blood. 2008;111(5):2866.
58. Cortés-Funes H, Coronado C. Role of anthracyclines in the era of targeted therapy. Totowa, N.J. :2007. p. 56-60.
59. Yaqub F. Mechanism of action of anthracycline drugs. Lancet Oncology. 2013;14(8):e296-e.
60. Weiss RB. The anthracyclines: will we ever find a better doxorubicin? Philadelphia1992. p. 670-86.
61. Foreningen for utgivelse av Norsk legemiddelhåndbok: Apotekforeningen Dnl, Helsedirektoratet, Nasjonalt kunnskapssenter for helsetjenesten, Statens legemiddelverk. Norsk legemiddelhåndbok for helsepersonell. 2013:128, 807-10.
62. Bardal SK, Waechter JE, Martin DS. Applied pharmacology: Elsevier Health Sciences; 2011.
63. Obrien MER, Wigler N, Inbar M, Rosso R, Grischke E, Santoro A, et al. Reduced cardiotoxicity and comparable efficacy in a phase III trial of pegylated liposomal doxorubicin HCl (CAELYXtrade;/Doxilsupldquo;/sup) versus conventional doxorubicin for first-line treatment of metastatic breast cancer. Annals of Oncology. 2004;15(3):440-9.

64. Minotti G, Menna P, Salvatorelli E, Cairo G, Gianni L. Anthracyclines: molecular advances and pharmacologic developments in antitumor activity and cardiotoxicity. Pharmacological reviews. 2004;56(2):185.

65. Than Htun M. Photophysical study on daunorubicin by fluorescence spectroscopy. 2009. p. 344-8.

66. Matos C, Moutinho C, Lobão P. Liposomes as a Model for the Biological Membrane: Studies on Daunorubicin Bilayer Interaction. The Journal of Membrane Biology. 2012;245(2):69-75.

67. Coukell A, Faulds D. Epirubicin. Drugs. 1997;53(3):453-82.

68. Marie C, Petri WA. Amoebic dysentery. London [England] :2013.

69. Radomski JL, Hagan EC, Fuyat HN, Nelson AA. The pharmacology of ipecac. The Journal of pharmacology and experimental therapeutics. 1952;104(4):421.

70. Khandelwal N, Chander Y, Rawat KD, Riyesh T, Nishanth C, Sharma S, et al. Emetine inhibits replication of RNA and DNA viruses without generating drug-resistant virus variants. Antiviral Research. 2017;144:196-204.

71. Akinboye ES, Rosen MD, Bakare O, Denmeade SR. Anticancer activities of emetine prodrugs that are proteolytically activated by the prostate specific antigen (PSA) and evaluation of in vivo toxicity of emetine derivatives. Bioorganic & Medicinal Chemistry. 2017;25(24):6707-17.

72. Graybeal J, Hurst G, Stoner J, Chu S. Spectroscopy: Encyclopedia Britannica; 2018 [cited 2019 May 12th]. Available from: https://www.britannica.com/science/spectroscopy.

73. Fischer K, Schmidt M. Pitfalls and novel applications of particle sizing by dynamic light scattering. Biomaterials. 2016;98:79-91.

74. Hassan PA, Rana S, Verma G. Making Sense of Brownian Motion: Colloid Characterization by Dynamic Light Scattering. Langmuir. 2015;31(1):3-12.

75. Binns C. Introduction to Nanoscience and Nanotechnology. Hoboken, NJ, USA: Hoboken, NJ, USA: John Wiley & Sons, Inc.; 2010.

76. Brownian motion. In: Gooch JW, editor. Encyclopedic Dictionary of Polymers. New York, NY: Springer New York; 2007. p. 131-2.

77. Leybold®. Scehmatic diagram of Brownian motion of moelcules https://www.leybold-shop.com/chemistry/catalogue-of-experiments-chemistry/general-and-inorganic-chemistry/material-properties/structure-of-matter/brownian-motion-of-smoke-particles/vc1-1-3-1.html [cited 2019 May 12th]. Available from: https://www.leybold-shop.com/chemistry/catalogue-of-experiments-chemistry/general-and-inorganic-

chemistry/material-properties/structure-of-matter/brownian-motion-of-smoke-particles/vc1-1-3-1.html.

78. Coglitore D, Edwardson SP, Macko P, Patterson EA, Whelan M. Transition from fractional to classical Stokes–Einstein behaviour in simple fluids. Royal Society Open Science. 2017;4(12).

79. Labrie A, Marshall A, Bedi H, Maurer-Spurej E. Characterization of Platelet Concentrates Using Dynamic Light Scattering. Transfus Med Hemother. 2013;40(2):93-100.

80. Stuart BH. Infrared Spectroscopy : Fundamentals and Applications. Chichester: Wiley; 2004.

81. Merck. Lipid Analysis with Direct Detect® Spectrometer 2019 [cited 2019 Feb 2nd]. Available from: http://www.merckmillipore.com/NO/en/life-science-research/protein-detection-quantification/direct-detect-spectrometer/applications/lipid-analysis/hGOb.qB.KHkAAAFB3eARRkxC,nav.

82. Lipids ARP. 840059 | Hydro Egg PC - L-α-phosphatidylcholine, hydrogenated (Egg, Chicken).

83. Kurien BT, Scofield RH. Western Blotting : Methods and Protocols. New York, NY: Springer New York : Imprint: Humana Press; 2015.

84. Faoro V, Becker K-F, Stanta G, Stanta G. Western Blotting. Berlin, Heidelberg: Berlin, Heidelberg: Springer Berlin Heidelberg; 2011. 271-4 p.

85. Mahmood T, Yang P-C. Western blot: Technique, theory, and trouble shooting. North American Journal of Medical Sciences. 2012;4(9):429-34.

86. Western Blot (Western hybridization). Encyclopedia of Genetics, Genomics, Proteomics and Informatics. Dordrecht: Springer Netherlands; 2008. p. 2101-.

87. Buxbaum E. Chromatography. Boston, MA: Boston, MA: Springer US; 2011. 147-62 p.

88. Coskun O. Separation techniques: Chromatography. Northern clinics of Istanbul. 2016;3(2):156.

89. Schure MR, Moran RE. Size exclusion chromatography with superficially porous particles. Journal of Chromatography A. 2017;1480:11-9.

90. Ho WF, Stuart B, Prichard ER. High performance liquid chromatography. Cambridge: Royal Society of Chemistry; 2003.

91. Chen X, Murawski A, Patel K, Crespi C, Balimane P. A Novel Design of Artificial Membrane for Improving the PAMPA Model. An Official Journal of the American Association of Pharmaceutical Scientists. 2008;25(7):1511-20.

92. Clemons K, Kretsch A, Verbeck G. Parallel artificial membrane permeability assay for blood–brain permeability determination of illicit drugs and synthetic analogues. Science & Justice. 2014;54(5):351-5.

93. Anthracyclines; Studies from University of Montreal Further Understanding of Anthracyclines (The human organic cation transporter OCT1 mediates high affinity uptake of the anticancer drug daunorubicin). Atlanta2016. p. 2481.

94. Corning®. Corning® Gentest™ Pre-coated PAMPA Plate System, with Lid, 1/Pack, 5/Case product sheet [cited 2019 May 12th]. Available from: https://ecatalog.corning.com/life-sciences/b2c/US/en/Microplates/Assay-Microplates/96-Well-Microplates/Corning%C2%AE-Gentest%E2%84%A2-Pre-coated-PAMPA-Plate-System%2C-with-Lid%2C-1-Pack%2C-5-Case/p/353015?lang=en.

95. Bennion BJ, Be NA, McNerney MW, Lao V, Carlson EM, Valdez CA, et al. Predicting a Drug's Membrane Permeability: A Computational Model Validated With in Vitro Permeability Assay Data. The journal of physical chemistry B. 2017;121(20):5228.

96. Creative Bioarray. Parallel Artificial Membrane Permeability Assay [cited 2019 May 11th]. Available from: https://www.creative-bioarray.com/Services/pampa-assay.htm.

97. Deng C-X. Conditional knockout mouse models of cancer. Cold Spring Harbor, NY :2014. p. 1217-33.

98. Rebe C, Ghiringhelli F. Cytotoxic effects of chemotherapy on cancer and immune cells: how can it be modulated to generate novel therapeutic strategies?(Report). 2015;11(19):2645.

99. Bjørnstad R, Aesoy R, Bruserud Ø, Brenner AK, Giraud F, Dowling TH, et al. A Kinase Inhibitor with Anti-Pim Kinase Activity is a Potent and Selective Cytotoxic Agent Toward Acute Myeloid Leukemia. 2019. p. 567.

100. MOLM13 product sheet: DSMZ; [cited 2019 May 11th]. Available from: https://www.dsmz.de/catalogues/details/culture/ACC-554.html.

101. ATCC®. NRK-49F (ATCC® CRL-1570™) product sheet [cited 2019 May 11th]. Available from: https://www.lgcstandards-atcc.org/products/all/CRL-1570.aspx#generalinformation.

102. ATTC®. H9c2(2-1) (ATCC® CRL-1446™) product sheet [cited 2019 May 11th]. Available from: https://www.lgcstandards-atcc.org/products/all/CRL-1446.aspx#generalinformation.

103. Merck. Cell Proliferation Reagent WST-1 product sheet [cited 2019 May 11th]. Available from: https://www.sigmaaldrich.com/catalog/product/roche/cellproro?lang=en&region=NO.

104. Koutsopoulos S. Peptide applications in biomedicine, biotechnology and bioengineering: Woodhead Publishing; 2017.
105. Fisher T. Hoechst 33342 Solution (20 mM) product sheet [cited 2019 May 11th]. Available from: https://www.thermofisher.com/order/catalog/product/62249.
106. Knudsen KS, Universitetet i Bergen Kjemisk i. Development of nanocarriers for co-delivery of statins and anthracyclines. Bergen: Department of Chemistry, University of Bergen; 2017.
107. Shanler M. Automation of Pre-coated PAMPA plate improves predictability, reproducibility and efficiency 2012 [cited 2019 May 25th]. Available from: https://www.corning.com/catalog/cls/documents/application-notes/an_DL_GT_053_Automation_of_Pre-coated_PAMPA_Plates_Improves_Predictability_Reproducibility_Efficiency.pdf
108. Santa Cruz Biotechnology. Caspase-3 Antibody (E-8): sc-7272 product sheet [cited 2019 May 13th]. Available from: https://www.scbt.com/scbt/product/caspase-3-antibody-e-8?productCanUrl=caspase-3-antibody-e-8&_requestid=13141713.
109. Erasmus M. Bortezomib (Velcade®): A feasibility and phase II study in childhood relapsed acute lymphoblastic leukemia.
110. Paszko E, Senge M. Immunoliposomes. Current medicinal chemistry. 2012;19(31):5239-77.
111. Gundersen ET, Universitetet i Bergen Kjemisk i. The production and characterization of drug-loaded liposomal and PLGA nanocarriers for targeted treatment of acute myeloid leukemia. Bergen: Department of Chemistry, University of Bergen; 2016.

Appendix I - Western blotting results

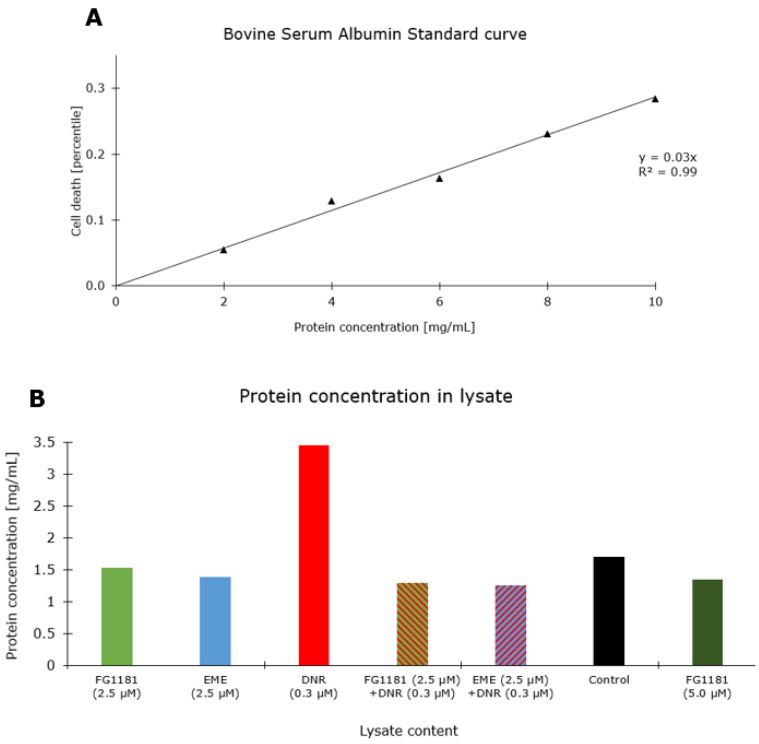

Figure App.I – Bradford assay for calculation of protein concentration in the lysates. A, The standard curve used to calculate protein concentration in the lysates. **B,** Protein concentration in the lysates used for Western blotting. Note that blotting was performed with two concentrations of FG1181.

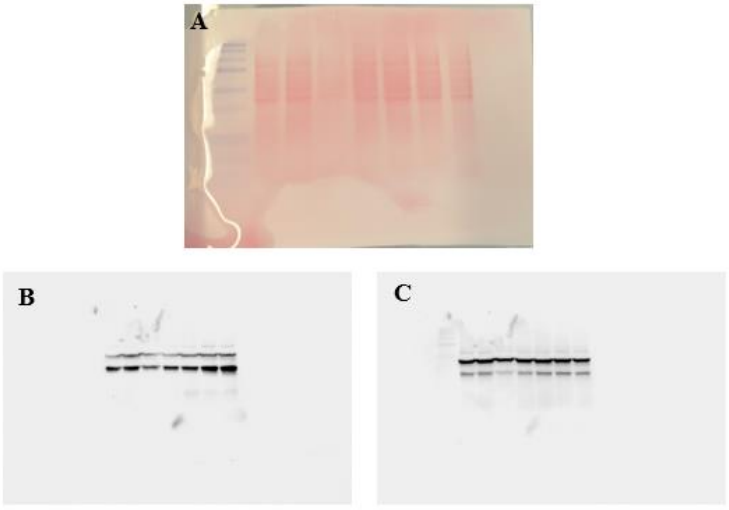

Figure App. II – Western blotting images: Images of bonds on the membrane. The bonds are placed in the same order as the column in App.I.. **A,** Image after Ponceau staining of the membrane. **B,** Caspase 3.**C**, β-actin.

Appendix II – RP-HPLC spectra of FG1181 and daunorubicin loaded liposomes

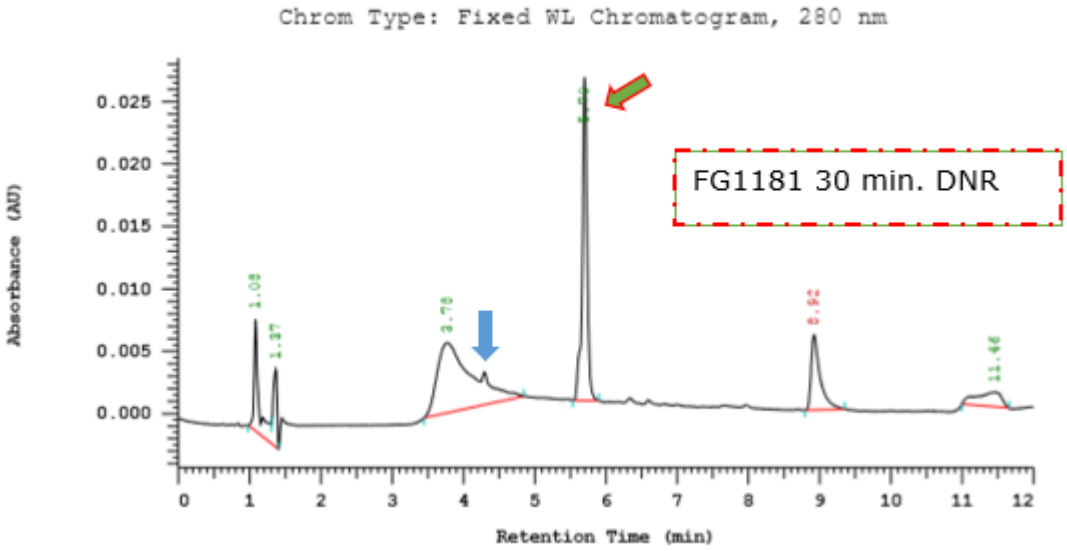

Figure App. III – RP-HPLC spectrum of FG1181 and Daunorubicin loaded liposomes form Batch B. The liposomes were loaded first with FG1181 for 30 minutes at 60°C and then DNR was added. Note the low emetine top marked with the blue arrow. The green and red arrow indicate FG1181 and DNR without base peak separation.